Top Curr Chem (2007) 271: 79–118
DOI 10.1007/128_070

Published online: 2 September 2006

Bio-inspired Crystal Growth by Synthetic Templates

Shu-Hong Yu

Division of Nanomaterials and Chemistry, Hefei National Laboratory for Physical Sciences at Microscale, School of Chemistry & Materials,
University of Science and Technology of China, Jinzhai Road 96, 230026 Hefei, China
shyu@ustc.edu.cn

Abstract Recent advances in bio-inspired strategies for the controlled growth of inorganic crystals using synthetic templates will be overviewed. There are a huge number of additives with different functionalities which can influence crystal growth; however, we only focus on the controlled growth and mineralization of inorganic minerals using synthetic templates as crystal growth modifiers, including biopolymers and synthetic polymers. New trends in the area of crystallization and morphogenesis of inorganic and inorganic–organic hybrid materials will be reviewed, including synergistic effects

of crystal growth modifiers in water and in a mixed solvent, and crystallization on artificial interfaces or within matrices. Combination of a synthetic template with a normal surfactant or crystallization in a mixed solution system makes it possible to access various inorganic crystals with complex form and unique structural features. Several different morphogenesis mechanisms of crystal growth, such as selective adsorption, mesoscopic transformations, and higher order assembly, will be discussed. In addition, crystallization on artificial interfaces including monolayers, biopolymer and synthetic polymer matrices for controlled crystal growth, and emerging crystallization on foreign external templates and patterned surfaces for creation of patterned crystals will also be overviewed.

Keywords Crystal growth · Crystallization · Biopolymer · Synthetic polymer · Interface · Matrix · Self-assembly

1 Introduction

Biominerals are well-known composites of inorganic and organic materials in the form of fascinating shapes and high ordered structures, which exist in Nature as, for example, oyster shells, corals, ivory, sea urchin spines, cuttlefish bone, limpet teeth, magnetic crystals in bacteria, and human bones, created by living organisms [1, 2]. During the past few decades, it has been one of the hottest research subjects in materials chemistry and its cutting-edge fields to explore new bio-inspired strategies for self-assembling or surface-assembling molecules or colloids to generate materials with controlled morphologies, unique structural specialty, and complexity [3–10, 12, 13]. Especially, learning from Nature on how to create superstructures resembling naturally existing biominerals with their unusual shapes and complexity has attracted a lot of attention [14–20]. Furthermore, exploration of rational methods for the synthesis of a rich family of functional inorganic crystals or hybrid inorganic/organic materials with specific size, shape, orientation, organization, complex form, and hierarchy has also attracted a lot of attention owing to their importance and potential applications in industry [21–32].

In recent years, several excellent reviews on biomineralization/crystallization with different viewpoints and focuses have been published [10, 33, 34]. For example, biomineralization of unicellular organisms with complex mineral structures from the viewpoint of molecular biology [33], generating new organized materials through the biospecific interaction and coupling of biomolecules with inorganic nanosized building blocks [34], producing single-crystal mosaics, nanoparticle arrays, and emergent nanostructures with complex form and hierarchy by mesoscale self-assembly and cooperative transformation, and reorganization of hybrid inorganic–organic building blocks [10]. In addition, advances in polymer controlled crystallization

and directed crystal growth, biomimetic mineralization, and synthesis of mesoscale order in hybrid inorganic–organic materials via nanoparticle self-assembly have been highlighted very recently [35–38].

In this review, the latest advances in the synthetic template controlled growth and crystallization of various inorganic minerals by bio-inspired approaches will be overviewed. The review is organized into five parts. First, general principles of crystal growth will be summarized (Sect. 2). Second, an overview of the recent advances in bio-inspired crystal growth of different inorganic crystals under the control of diverse biopolymers and synthetic templates will be summarized (Sect. 3). Emerging crystallization approaches and synergistic effects of crystal growth modifiers such as by a combination of polymers, or the combination of a polymer with low-mass surfactant molecules, as well as crystallization in a mixture of solvents, will be overviewed (Sect. 4). The diverse crystallization events occurring on the interfaces/substrates or within artificial matrices, and on emerging patterned crystallization will be overviewed (Sect. 5). Finally, we will give a summary and perspectives on this active research area (Sect. 6).

2
Basic Principles of Crystal Growth

2.1
Crystal Growth Habit and Crystal Shape

It is well known that diverse crystal shapes of the same compound are due to the differences of the crystal faces in surface energy and external growth environment [39]. Basically, crystal shape is determined by crystal habit and branching growth [39–45]. Crystal habit is determined by the relative order of surface energies of different crystallographic faces of a crystal [39–41], and in fact the shape of a crystal is usually the outside embodiment of its intrinsic cell replication and amplification. Branching growth created by a diffusion effect [42, 43] also plays an alternative role in the crystal shape due to the fact that the consumption of the ions or molecules near the surface of a growing crystal will form a concentric diffusion field around the crystal [44, 45]. This makes the apexes of a polyhedral crystal, which protrude further into the region of higher concentration, grow faster than the central parts of facets, thus forming branches [46].

As early as 1901, Wulff described a thermodynamic treatment of the crystal shape changes based on an energy minimized total surface area [39]. It is nowadays well known that this purely thermodynamic treatment cannot always predict the crystal shape, because crystallization and crystal shape often also rely on kinetic effects and defect structures like screw dislocations or kinks etc. The specific adsorption of ions or organic additives to particu-

lar faces can inhibit the growth of these faces. Generally, the growth rate of a crystal face is usually related to its surface energy if the same growth mechanism acts on each face. The fastest crystal growth will occur in the direction perpendicular to the face with the highest surface energy in order to eliminate or reduce higher energy surfaces, while lower energy surfaces will become more exposed in area. Thus, the fast growing faces usually have high surface energies and finally they will vanish in the final shape (Fig. 1a).

Crystal growth habit can be modified when the relative order of surface energies can be changed or when crystal growth along certain crystallographic directions is selectively hindered by a crystal growth modifier [4]. In the pres-

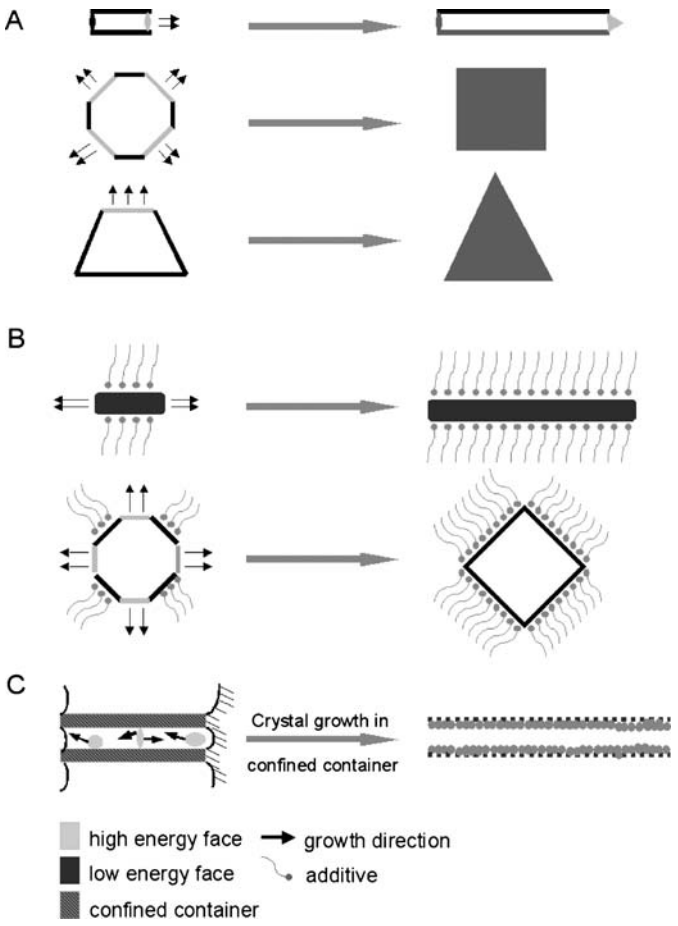

Fig. 1 Illustration of the crystal growth process. **a** Normal crystal habit in the absence of crystal modifiers; **b** the altered crystal growth habit due to the selective/preferential adsorption of crystal modifiers to a specific crystallographic face; and **c** the crystal growth within an confined environment

ence of crystal growth modifiers, the preferential/selective adsorption of crystal modifiers to a specific crystallographic face becomes stronger than that of others due to the anisotropy in adsorption stability decreasing the surface energy of the adsorbed face and inhibiting the crystal growth perpendicular to this face, thus altering the final shape of the crystal (Fig. 1b) [32, 47]. In addition, the crystal shape can be altered if the growth process occurs in a confined environment (Fig. 1c). The general crystal growth mechanisms in solution will be discussed in the following section.

2.2 Crystal Growth Mechanisms in Solution

The crystal growth mechanisms in solution are rather complicated and there are several that dominate the crystal growth process in the solution system. Recently, the classical and nonclassical crystallization mechanisms of inorganic minerals in solution systems have been described according to the latest developments in the crystallization field, as illustrated in Fig. 2 [35].

Primary nanoparticles are nucleated from the clusters called "critical crystal nuclei" which are the smallest crystalline units capable of further growth. Further growth of these primary nanoparticles by ion attachment and unit cell replication results in the formation of a final macroscopic single crystal, which is more or less an amplification of the initial crystal (Fig. 2a) [35].

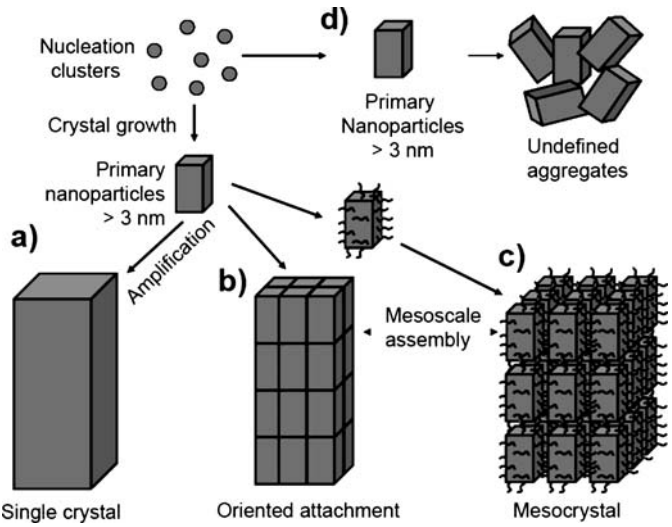

Fig. 2 **a** Classical and **b**, **c** nonclassical crystallization mechanisms via self-assembly. Crystallization starts from nucleation clusters (*upper left*). **d** The primary nanoparticles can also grow by ion attachment, but they then aggregate uncontrollably at a certain stage, forming undefined polycrystalline aggregates. (Reproduced from [35], © 2005, MRS)

These primary nanoparticles can also grow further into a single crystal by so-called oriented attachment of these nanoparticles [48–52] because their surfaces contain face-specific information (Fig. 2b). In addition, face-specific interactions between these primary building units can undergo directed self-assembly, resulting in a so-called mesocrystal [53], which is usually an intermediate on the formation pathway of a single crystal (Fig. 2c). These primary units can also grow by ion attachment alone, with unit cell replication, but they then aggregate at a certain stage, forming undefined polycrystalline aggregates (Fig. 2d).

Usually, more complex and emergent superstructures cannot be simply grown/constructed via a simple unit cell amplification process; instead they are normally formed via spontaneous self-organization of nanobuilding units carried with face-specific information in a controlled way and complicated mesoscale transformation mechanisms. The shape of crystals can be altered by various additives, i.e., inorganic cations and anions, organic additives, or even solvents, which has been overviewed recently [54]. In the following sections, we only focus on the latest developments in the emerging field of bio-inspired crystal growth of various inorganic crystals under the control of synthetic templates, including biopolymers, diverse synthetic polymers and their synergistic effects, and crystallization on artificial interfaces or within artificial matrices.

3
Synthetic Template Controlled Crystal Growth

Bio-inspired approaches for mimicking the biomineralization process of biominerals have been intensively studied. Usually, the synthetic templates used for these approaches include biopolymers and synthetic polymers. There are a huge number of synthetic polymers used for this purpose, including polyelectrolytes, graft copolymers, block copolymers, dendrimers, and foldamers.

The principle of controlled crystallization and morphosynthesis using a soluble polymer as crystal growth modifier in a solution which does not form an assembly is completely different from the templating effects, such as artificial interfaces and matrices or patterned substrates, which will be discussed in Sect. 5. The structure setup and evolution certainly does not rely on transcription or a straightforward template effect, but relies on a synergistic effect of the mutual interactions between functional groups of the polymers and inorganic species, and the subsequent reconstruction by a self-assembly process [4, 10, 55].

In the following sections, we will discuss recent advances in the area of polymer controlled crystal growth and morphogenesis of various inorganic minerals by the use of biopolymers, various synthetic polymers, and non-

classical block copolymers—-so-called double-hydrophilic block copolymers (DHBCs) [35–37].

3.1 Biopolymers

Biopolymers consist of unique self-assembled structures and thus are often used as a natural soluble additive for the morphogenesis of complex superstructures. So far, in vitro experiments have failed to reproduce the complex biomineral shapes such as $CaCO_3$ by the use of a variety of additives such as dextran [56], collagen [57], soluble mollusk shell proteins extracted from nacre [58, 59], soluble macromolecules extracted from coralline algae [60], soluble macromolecules extracted from the respective layers of a mollusk shell [61, 62], protein secondary structures [63], and peptides for $CaCO_3$ crystallization [64]. The reason is that the biomineralization process is very complicated and an insoluble matrix can also influence the crystallization location as a compartment (Sect. 5).

The concept of using biopolymers for crystallization/mineralization has been widely expanded to synthesize and assemble different kinds of other functional inorganic nanostructures in recent years, which has been overviewed recently [35, 38, 54, 65] with specific examples. Directed assembly and organization through the interaction of biomolecule templates, such as DNA [66–69], virus [70], tobacco mosaic virus [71], and peptide [72], with inorgainc species like Au and ZnS make it possible to access organized nanostructures with different shape and dimensionalities. Magnetic crystals such as tabular single-domain magnetite [73] and a regulated cubic shape [74] can be grown at room temperature in water with close to neutral pH by biological methods. Some kinds of magnetotactic bacteria can synthesize and align ferromagnetic mineral greigite, as demonstrated by Mann et al. [75]. Sastry and coworkers have used fungi and actinomycetes, which can produce CO_2 during their growth, to form metal carbonate [76–79]. The same group has used the extracts of the lemongrass plant and of *Azadirachta indica* leaf to react with aqueous noble metal ions to produce thin, flat, single-crystalline gold nanotriangles [80], and silver and bimetallic Au/Ag nanoparticles [81].

The complex morphology of the nanopatterned silica diatom cell walls has been found to be related to species-specific sets of polycationic peptides, so-called silaffins, which were isolated from diatom cell walls [82]. The morphologies of precipitated silica can be controlled by changing the chain lengths of the polyamines as well as by a synergistic action of long-chain polyamines and silaffins [83, 84]. It has been proposed that the delicate pattern formation in diatom shells can be explained by phase separation of silica solutions in the presence of these polyamines [85]. Various linear synthetic analogs of the natural active polyamines in biosilica formation can accelerate the silicic acid condensation even more than the above mentioned

silaffins [86]. Block copolypeptide poly(L-cysteine$_{30}$-*b*-L-lysine$_{200}$) has been used for biosilification [87]. Similar to the silaffins, silicateins can also catalyze the formation of silica at ambient conditions, but from tetraethoxysilane (TEOS) rather than silicic acid [88].

3.2 Synthetic Polymers

3.2.1 Polyelectrolytes

Simple low molecular mass polyelectrolytes can electrosterically stabilize inorganic colloids. Besides this function, low molecular mass polyelectrolytes have been widely used as additives in the controlled growth of diverse inorganic materials [35, 38]. The addition of polyelectrolytes with strong inhibition ability can stabilize the amorphous nanobuilding blocks in the early stage, and then stimulate a mesoscale transformation [10] or act as a material depot in a dissolution–recrystallization process. Time-resolved study of the scale inhibition efficiency of polycarboxylates has shown that amorphous precursor particles were formed in the initial stages [89] and were also observed in other cases.

For example, poly(acrylic acid) or poly(aspartic acid) crystal growth modifiers or structure directing agents can be used to induce the formation of various kinds of complex and hierarchical superstructures, such as structured calcium phosphate [90], helical $CaCO_3$ [91, 92], complex spherical $BaCO_3$ superstructures [93], hollow octacalcium phosphate ($Ca_8H_2(PO_4)_6 \cdot H_2O$) [94], $BaSO_4$ [95] and $BaCrO_4$ fiber bundles, or superstructures with complex repetitive patterns [96] as shown in Fig. 3.

The formation mechanism of the complex structures under control of a polyelectrolyte has not yet been well understood. Unusual complex structures of calcite helices or hollow helices can be obtained in the presence of a chiral polyaspartate, which can produce helical protrusions or occasionally hollow helices as shown in Fig. 3a [91]. Gower and colleagues have proposed a so-called polymer-induced liquid precursor (PILP) process to illustrate the possible mechanism for the formation of the complex morphologies [92]. In this process, it is believed that the addition of small amounts of polymer ($\mu g\,mL^{-1}$ range) to the crystallizing solution results in the formation of a liquid–liquid phase separation to precursor droplets, which can adapt complex shapes before they crystallize. Yet, the formation mechanism of such amazing spherulitic vaterite aggregates with helical structures and with spiral pits is still not clear. $CaCO_3$ mineralization in the presence of collagen via a PILP process can result in the formation of fibrous aggregates [97]. Recently, Gower et al. demonstrated that rhombohedral calcite crystals grown in the absence of polymeric additives can be introduced into the above PILP process

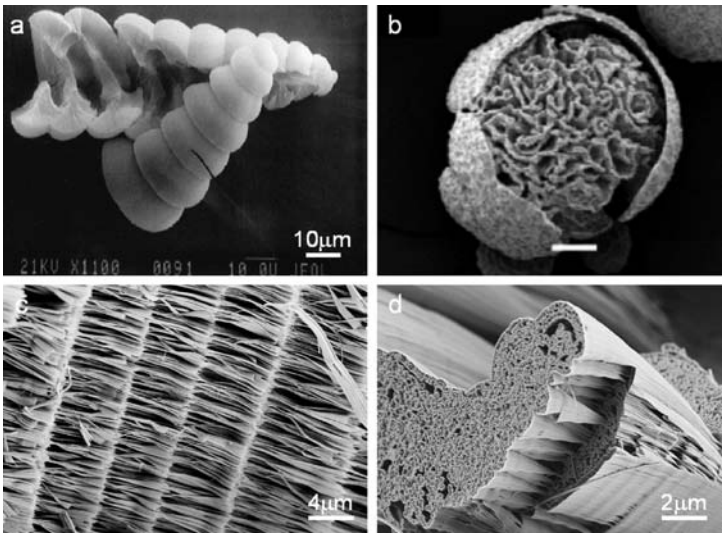

Fig. 3 Complex form of inorganic minerals formed by crystallization under control of a simple polyelectrolyte. **a** Helical $CaCO_3$ structures produced by the PILP process. Occasionally, the helices are partially hollow. The hollow helix fractured by micromanipulation. The *scale bar* represents 10 μm. (Reproduced from [91], © 1998, Elsevier Sciences). **b** Scanning electron microscopy (SEM) image of octacalcium phosphate (OCP)–polyelectrolyte architectures synthesized in the presence of polyaspartate, and isolated after different periods of aging, in solution for 3 h. The *scale bar* represents 100 μm. (Reproduced from [94], © 2002, Wiley). **c**,**d** Complex forms of $BaSO_4$ bundles and superstructures produced in the presence of 0.11 mM sodium polyacrylate (M_n = 5100), at room temperature, $[BaSO_4]$ = 2 mM, pH = 5.3, 4 days. **c** The detailed superstructures with repetitive patterns. (Reproduced from [96], © 2003, American Chemical Society). **d** A zoomed SEM image of the well-aligned bundles. (Reproduced from [37], © 2005, MRS)

to act as seeds, and to induce the growth of crystalline calcite fibers on the surface by selective deposition of the PILP film on top of the rhombohedra rather than on the surrounding glass substrate [98] (Fig. 4). A liquid-phase mineral precursor, the so-called bobble head formed under physiological conditions (and down to temperatures as low as 4 °C), was observed on the tips of fibers, suggesting that an analogous solution–precursor–solid (SPS) mechanism may act in this system, which is quite similar to the vapor–liquid–solid (VLS) [99] and solution–liquid–solid (SLS) mechanisms [100] proposed for the growth of one-dimensional fibers under hot conditions.

The observed thin porous membrane of oriented octacalcium phosphate (OCP, $Ca_8H_2(PO_4)_6 \cdot H_2O$) crystals (Fig. 3b) on the outside of hollow OCP crystals mineralized in the presence of polyaspartate could be similar to that observed in the case of mineralization of $CaCO_3$ by a typical PILP process [92, 97].

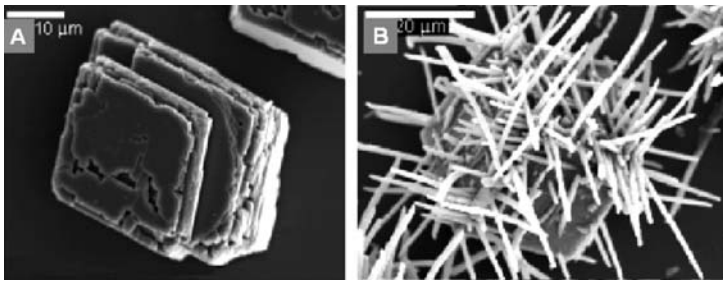

Fig. 4 SEM micrographs of calcium carbonate deposited onto rhombohedral substrate crystals in the presence and absence of micromolar amounts of acidic polymer. **a** Calcite overgrowth on calcite substrates in the absence of polymeric additives. The *scale bar* represents 10 μm. **b** Calcite fibers grown on a solution-grown calcite substrate. In this case, the fibers appear to exhibit an isoepitaxial relationship with the underlying substrate crystal. The *scale bar* represents 20 μm. (Reproduced from [98], © 2004, American Chemical Society)

By crystallization of $BaSO_4$ and $BaCrO_4$ minerals using the sodium salt of poly(acrylic acid) as crystal modifier, elegant nanofiber bundles and their superstructures with conelike crystals [95] and hierarchical and repetitive growth patterns can be generated [96] (Fig. 3c,d), possibly based on a self-limiting growth mechanism. In this mechanism, a dipole crystal may be favored for a heterogeneous nucleation as one end of the crystal is determined by the heterogeneous surface instead of homogeneous solution and the other by the solution/dispersion [101]. A new heterogeneous nucleation event will occur on the rim of the mother crystal to start a self-limiting growth process, which is favorable for the formation of repeated patterns and a "cone-in-a-cone" superstructure (Fig. 3c,d). The low molecular weight polyelectrolytes poly(allylamine hydrochloride) (PAH) and poly(sodium 4-styrenesulfonate) (PSS) were also used for the mineralization of complex spherical $BaCO_3$ superstructures made of rodlike crystals [93], spherical $CaCO_3$ particles [102], and a hydroxyapatite/PAH–PSS polyelectrolyte composite shell [103]. Recently, unusual $CaCO_3$ superstructures, which transformed from the typical calcite rhombohedra to rounded edges, to truncated triangles, and finally to concavely bent lenslike superstructures using PSS as crystal modifier, were generated by a nonclassical crystallization process [104], where PSS can bind selectively to the otherwise nonexposed (001) calcite face, resulting in mesostructures composed of truncated triangular units instead of the typical rhombohedra.

Poly(L-isocyanoalanyl-D-alanine) with a regular distribution of carboxylic acid-terminated side chains was taken as a model template to investigate the relation between the structure of a polymeric template and a developing calcite phase [105]. A series of carboxylate-containing polyamides were synthesized [106–108] for the purpose of crystallization of $CaCO_3$. Helical

calcite superstructures, with the helix turn corresponding to the copolymer enantiomer of chiral copolymers of phosphorylated serine (Ser) and aspartic acid (Asp) with molar masses 15 000–20 000 g mol^{-1}, could be generated under a limited experimental window [109] when a high degree of phosphorylated Ser (75 mol %) and 25 mol % Asp in the copolymer were applied.

Recently, $CaCO_3$ microspheres composed of vaterite nanoparticles with a size of 15–25 nm were mineralized by a simple polypeptide-directed strategy using sodium poly(aspartic acid) (M_w = 14 900) as an additive, and a remarkably soft nature of the nanoparticle assembly was found [110]. In addition, a family of superstructured vaterite mesocrystals, with hexagonal symmetry and uniform size and shape, could be mineralized by a vapor diffusion technique in the presence of an *N*-trimethylammonium derivative of hydroxyethyl cellulose [111]. Stable amorphous $CaCO_3$ hollow spheres have been synthesized using phytic acid as an additive [112], which is rich in phosphate groups and shows strong inhibiting ability for amorphous $CaCO_3$. The diameter of the amorphous $CaCO_3$ spheres could be controlled by adjusting the concentration of phytic acid [112].

Polyacrylamide (PAM) and carboxyl-functionalized polyacrylamide (PAM-COOH) were used as additives to selectively grow hexagonal ringlike ZnO structures and very thin discoid-like microstructures under mild conditions [113] (Fig. 5). The preferential and selective adsorption of polyacrylamide molecules on the (002) basal plane strongly inhibits the growth along this direction. In addition, the polymer occluded within the hybrid aggregates formed in the initial stage will undergo adsorption and desorption, and a polymer concentration gradient will form from the inside to the outside of the hybrid particle containing multiple chelating units. In this process, the dissolution of the core part of the crystal will occur to form ringlike struc-

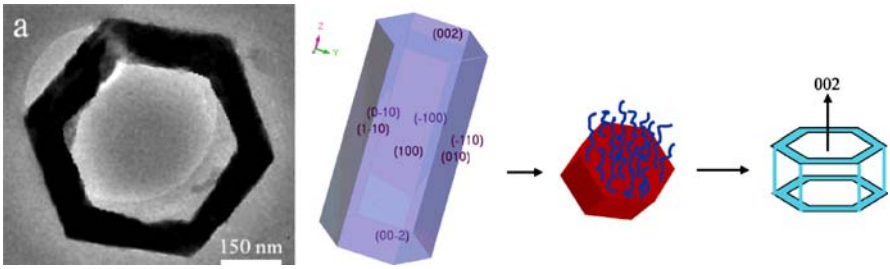

Fig. 5 **a** Transmission electron microscopy (TEM) image of a single ZnO nanoring formed in the presence of PAM. Modeling the morphology and growth habit of ZnO crystals in the absence of any external influence (*left*, simulated with the Cerius2 software), polymer adsorbed on (002) faces of ZnO (*middle*), and the final ZnO nanoring formation in the presence of PAM macromolecules (*right*). (Reproduced from [113], © 2006, American Chemical Society)

tures, as recently proposed in a block copolymer controlled crystallization of hollow $CaCO_3$ microrings (described in Sect. 3.2.3).

Imai et al. reported that poly(acrylic acid) (PAA) molecules with carboxy groups behave as a suppressant and template for the crystallization of calcium carbonate [114]. The results demonstrated that high molecular weight PAAs anchored to a glass surface promoted the oriented nucleation of calcite crystals. The combination of low and high molecular weight PAAs can achieve a moderate suppression effect, resulting in the formation of lozenge-shaped films consisting of iso-oriented crystal grains.

3.2.2 Graft Copolymers

Only a few examples have been demonstrated for crystallization control in aqueous environments using double hydrophilic graft copolymers [115] as reviewed previously [35]. Wegner and colleagues prepared poly(ethylene oxide) graft copolymers with methacrylic acid and/or vinylsulfonic acid by free radical polymerization [115], which have been applied to controlling the crystallization of ZnO [115]. In addition, poly(ethylene oxide) graft copolymers with a polyacetal backbone and functional carboxy groups along the main chain have been prepared [116], which were used as additives in the crystallization of $CaCO_3$ [117].

3.2.3 Block Copolymers

Block copolymers with hydrophilic and hydrophobic blocks show a similar behavior to low molecular weight surfactants [118, 119]. In recent years, various kinds of block copolymers have been used for controlled crystallization and stabilization of nanoparticles [35]. Among them, a new class of functional polymers, the so-called double-hydrophilic block copolymers (DHBCs), have been designed as crystal modifiers for mimicking the biomineralization process [35]. Typically, a DHBC consists of one hydrophilic block designed to interact strongly with the appropriate inorganic minerals and surfaces, and another hydrophilic block that does not interact (or only weakly interacts) and mainly promotes solubilization in water. Recently, progress has demonstrated that the DHBCs are very effective in crystallization control of various minerals [35, 36]. These polymers are designed to have typically rather small block lengths of 10^3–10^4 g mol^{-1}. The solvating block shows good solubility in water and is in most cases a poly(ethylene oxide) (PEO) block and the binding block contains variable chemical patterns, which show strong affinity to minerals and have a strong interaction with inorganic crystals. The functional groups on the binding block usually include – OH, – COOH, – SO_3H, – SO_4, – PO_3H_2, – PO_4H_2, – SCN, – NR_3, – HNR_2, and – H_2NR [35].

Usually, DHBCs are used as excellent stabilizers for the in situ formation of various metal nanocolloids and semiconductor nanocrystals such as Pd, Pt [120–122], Au [120–123], Ag [124], CdS [125], and lanthanum hydroxide [126]. It has been shown that DHBCs [127, 128] can exert a strong influence on the morphogenesis of a variey of inorganic particles such as $CaCO_3$ [129–137], $BaCO_3$, $PbCO_3$, $CdCO_3$, $MnCO_3$ [136], calcium phosphate [138], barium sulfate [139–142], barium chromate [101, 143], barium titanate [144], calcium oxalate dihydrate [145], zinc oxide [132, 146–149], cadmium tungstate [150], and chiral organic crystals [151], and can act as a template for silica formation [152] and even control the structure of ice and water [153]. DHBCs can be used for the stabilization of specific planes of some crystals for their oriented growth such as Au [123], ZnO [146–148], calcium oxalate [145], $PbCO_3$ [136], and $BaSO_4$ [141].

Recent advances have demonstrated that DHBCs can act as an excellent stabilizer and crystal growth modifier for the formation of various inorganic crystals with interesting shapes, stabilize specific crystal faces, control crystal polymorphism by polymer adsorption, and mediate the mesoscopic transformation and higher order assembly of nanoparticles as reviewed recently [36–38]. In the following part, we emphasize the latest progress and new examples on the controlled growth of unusual superstructures of complex form, and illustrate the extraordinary ability, flexibility, and versatility of the DHBCs in the controlled growth of mineral superstructures.

A rigid DHBC-poly(ethylene glycol)-*b*-poly(1,4,7,10,13,16-hexaazacyclooctadecane ethylene imine) has been used as a crystal modifier to mineralize $CaCO_3$ crystals called "pancakes" with a shape similar to the layered struc-

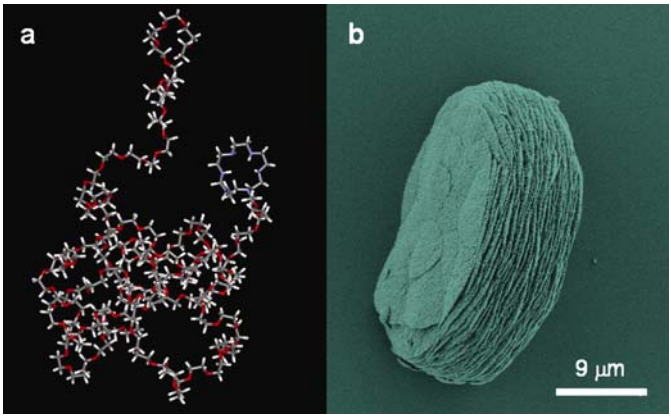

Fig. 6 **a** The structure of PEG-*b*-hexacyclen. **b** A typical SEM image of a pancake-like self-stacked $CaCO_3$ obtained after 2 weeks gas diffusion reaction in the presence of $1\,g\,L^{-1}$ PEG-*b*-hexacyclen, starting pH 4, $[Ca^{2+}] = 10\,mM$. (Reproduced from [154], © 2005, Wiley)

ture of nacre in *Haliotis rufescens*, as shown in Fig. 6 [154]. Layered crystals with different morphologies and surface structures, even disklike crystals, can be obtained by altering the mineralization conditions in the system. This study suggested that the morphologies of the crystal were not influenced by epitaxial match between the polymer and crystal faces, but that particle stabilization, crystallization time, time for polymer rearrangement, and surface ion density were of great effect on the resulting morphology [154].

Recently, a hydrophobically modified DHBC, poly(ethylene glycol)-*block*-poly(ethylene imine)-poly(acetic acid) (PEG-*b*-PEIPA), with on average one hydrophobic moiety at the end of the branched poly(ethylene imine) domain (PEG-*b*-PEIPA-C_{17}; PEG = 5000 g mol^{-1}, PEIPA = 1800 g mol^{-1}) [155] was found to form aggregates in aqueous solution, and showed an amazing texture and morphology control on the formation of unusual $CaCO_3$ microrings [156] (Fig. 7). It was proposed that the formation of $CaCO_3$ microrings is driven by the aggregation of polymer–inorganic hybrid nanocrystallites following crystallization inside unstructured polymer aggregates and the subsequent dissolution of nanocrystals from the inner side of the aggregates toward the outside. The hybrid core part of the disk is composed of primary nanocrystals with a large amount of attached polymer, which will have a great tendency to dissolve the $CaCO_3$ nanocrystals due to the large number of included multiple chelating ethylenediamine tetraacetic acid (EDTA) moieties from the block copolymer aggregates. This preferred dissolution event from the center of hybrid particles is similar to the formation of hollow $CaCO_3$ spheres under the control of a strongly chelating PEO-*b*-PEIPA additive, just without the hydrophobic tails [129]. This was also confirmed by a default experiment which showed that the rhombohedral calcite crystals formed in the absence of polymer were indeed dissolved in this polymer solution [156]. The formation of a polymer concentration gradient from the inside to the outside of the hybrid particle contained multiple chelating units, and the following restructuring within the hybrid structures, could be a reasonable and new explanation for such selective dissolution of the center of

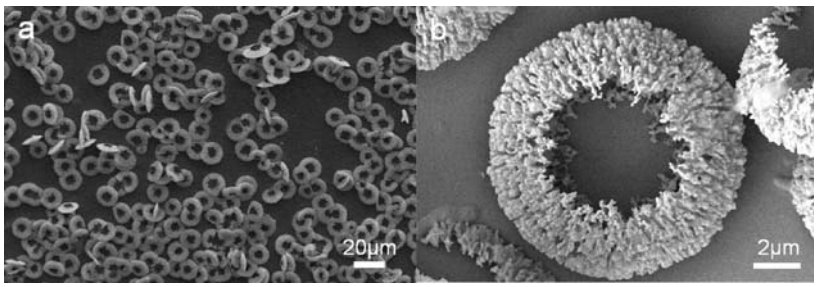

Fig. 7 SEM images of $CaCO_3$ microrings; 2.0 g L^{-1} PEG-*b*-PEIPA-C_{17}, 15 days, starting pH 4, [$CaCl_2$] = 20 mM. (Reproduced from [156], © 2006, American Chemical Society)

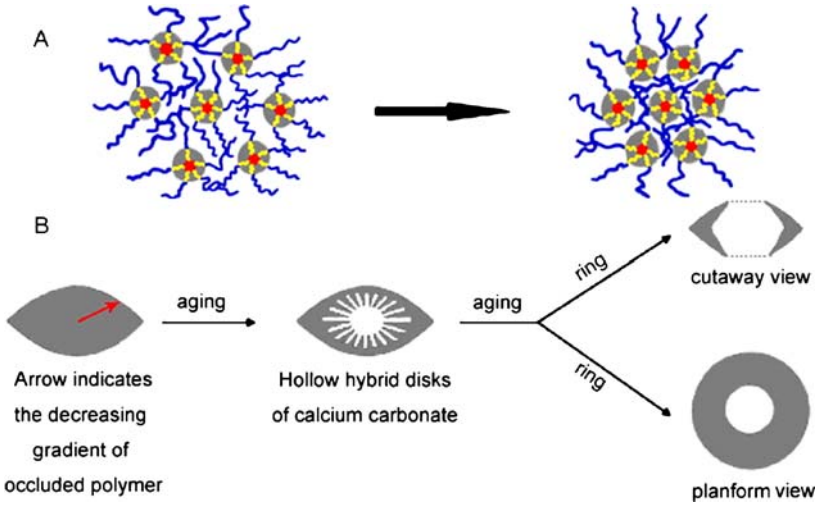

Scheme 1 **a** Aggregation mode of interlayer micelle-occluded nanocrystals. **b** Graphic presentation of the formation mechanism of $CaCO_3$ mesorings. *Gray*, calcium carbonate; *red*, hydrophobic block; *blue*, soluble neutral block; *yellow*, charged block. The *red arrow* indicates the decreasing gradient of occluded polymer within the disklike structure. (Reproduced from [156], © 2006, American Chemical Society)

the particles. This concept could also be helpful for the explanation of $CaCO_3$ hollow spheres [129] and amorphous $CaCO_3$ [112], and ZnO rings [113] by a polymer controlled crystallization process.

Recently, a racemic phosphonated DHBC, poly(ethylene glycol)-*b*-[2-(4-dihydroxyphosphoryl)-2-oxabutyl] acrylate ethyl ester (PEG-*b*-DHPOBAEE), was synthesized and applied to the controlled crystallization of $BaCO_3$ mineral. The chemical structure and a computer modeling structure of the functional head oligo[2-(4-dihydroxyphosphoryl)-2-oxabutyl] acrylate ethyl ester were depicted, showing its conformation of minimal energy in the absence of solvent (upper part in Fig. 8). It shows that this functional block is sterically overcrowded and adopts a stretched conformation, but with a high density of binding sites with mutual distances of 5–11 Å, implying a multiplicity of potential binding interactions with the inorganic crystal faces. Amazing $BaCO_3$ mineral helices have been successfully produced by programmed self-assembly of the elongated orthorhombic $BaCO_3$ units, based on the selective adsorption of PEG-*b*-DHPOBAEE onto the (110) faces of orthorhombic $BaCO_3$ (Fig. 8) [157]. This tectonic arrangement via coded self-assembly relies on two processes [157]: (1) the adsorption of the stiff DHBC onto the favorable (110) sites results in a staggered arrangement of aggregating nanoparticles that is controlled in direction after the aggregation of the first three particles, and (2) a particle approaching an aggregate in the perpendicular direction is presented with favorable and unfavorable adsorption

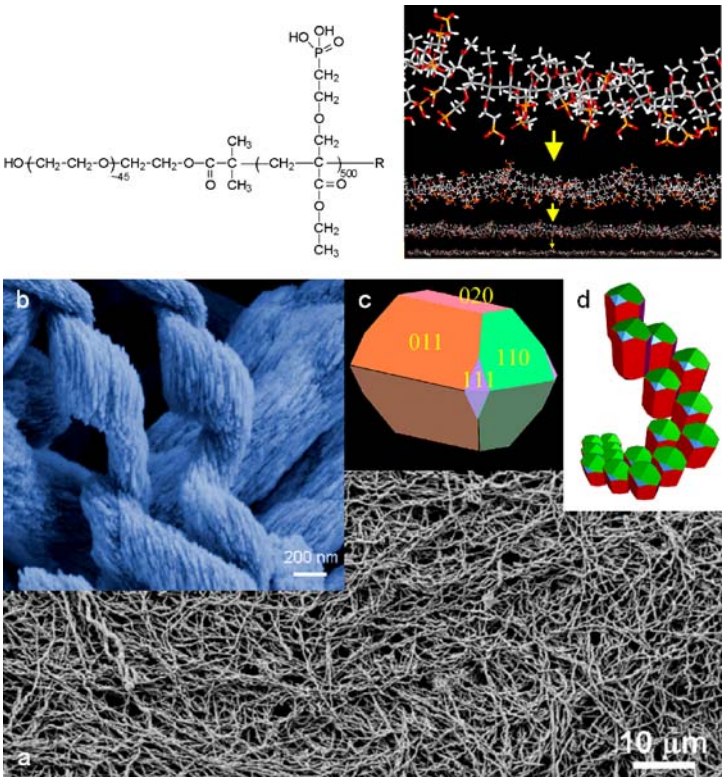

Fig. 8 *Top (left)*: Chemical structure of PEG-*b*-DHPOBAEE where R is either another PEG block or a hydrogen atom depending on the termination mode during polymerization. *Top (right)*: Different magnifications of the computer modeling results of the vacuum energy minimum conformation of the functional block of PEG-*b*-DHPOBAEE with 640 monomer units in vacuum. Note the stiff structure as a result of steric constraints. The modeling for the 640-mer was done with the *Cerius2* software (Accelrys). *Red*: O; *yellow*: P; *gray*: C; *white*: H. *Bottom*: **a** Helical $BaCO_3$ nanoparticle superstructures grown via a programmed self-assembly of elongated nanoparticles at room temperature using PEG-*b*-DHPOBAEE as template; 1 g L^{-1}, starting pH 4, [$BaCl_2$] = 10 mM. **b** Magnified SEM image showing the helical structure. **c** The primary nanocrystalline witherite building block in vacuum not representing observed face areas in solution but just illustrating the orientation of the relevant faces. **d** Proposed formation mechanism of the helical superstructure. (Reproduced from [157], © 2005, Nature Publishing Group)

sites, leading to a twist in the particle aggregate. The overlay of these two processes leads to helix formation (bottom part in Fig. 8). This successful access to inorganic helices demonstrated the possibility of selectively adsorbing additives onto specific crystal surfaces, and initiating the occurrence of the most advanced ways of so-called programmed self-assembly of nanoparticles, which can be used for the synthesis of various inorganic structures with unique structural features.

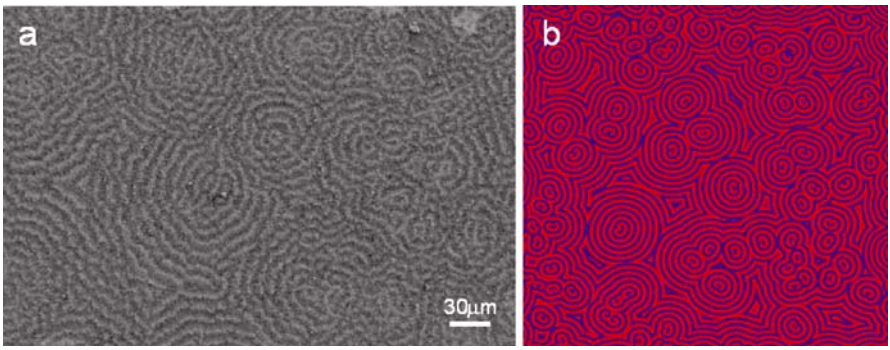

Fig. 9 **a** SEM images of the obtained concentric circle pattern of $BaCO_3$ crystals grown for 1 day; [polymer] = 1 g L^{-1}, [Ba^{2+}] = 10 mM, starting pH = 5.5. **b** Simulation result with a modified Brüsselator model for the reaction–diffusion equations. (Reproduced from [158], © 2006, Wiley)

Very recently, the polymer PEG-*b*-DHPOBAEE has also been used for mineralization of $BaCO_3$ mineral to spontaneously form a concentric circle Belousov–Zhabotinsky pattern made of $BaCO_3$ nanorods in solution on a glass substrate [158]. The experimental evidence indicated that the formation of the Ba–polymer complex precursor played a key role in the autocatalytic precipitation reaction and happened in a reaction–diffusion system, resulting in the spontaneous formation of micrometer-sized periodic rings of nanocrystalline $BaCO_3$ grown on the substrate in an aqueous solution [158]. The distance between adjacent rings is almost constant (ca. 5 μm) (Fig. 9a). The numerical simulations using a Brüsselator model for the reaction–diffusion equations qualitatively fit the observed oscillating precipitation reaction well (Fig. 9b). This amazing pattern formation underlies the fact that it is possible to form a spontaneously self-organized pattern in solution by a mesoscale transformation process, which is similar to the patterns observed in a variety of physical, chemical, and natural systems.

3.2.4 Dendrimers

Previously, dendrimers were used as organic matrices for the synthesis of a variety of inorganic nanomaterials and inorganic–organic composites [36, 159]. Dendrimers with different generations have been discovered as active additives for the controlled crystallization of $CaCO_3$ [159, 160]. It has been demonstrated that anionic starburst dendrimers can stabilize spherical vaterite particles for up to a week with controllable particle size in the range of 2.3–5.5 nm in dependence on the dendrimer generation number [161]. In addition, the combination of poly(propylene imine) dendrimers with oc-

tadecylamine can stabilize kinetically formed amorphous calcium carbonate (ACC) for periods exceeding 2 weeks in water [162, 163].

3.2.5
Foldamers

Recently, a simple oligopyridine foldamer was designed to recognize the surface of calcite through three carboxylates, projected from one face of the molecule [164]. At low concentrations of the trimer, elongated calcite crystals with angular, toothlike growth, identified as $\{\bar{1}\,01\}$ faces, were exclusively formed. The ordered array of carboxylates in the foldamer structure exerts a strong influence on the shape of growing calcite crystals via a specific interaction between the foldamer and the newly expressed faces of the growing calcite crystals.

3.2.6
Supramolecular Functional Polymer

Supramolecular directed self-assembly of inorganic and inorganic–organic hybrid nanostructures has emerged as an active area of recent research. The recent advance shows a remarkable feasibility to mimic natural mineralization systems by a designed artificial organic template, where a supramolecular functional polymer can be directly employed as mineralization template for the synthesis of novel inorganic nanoarchitectures [165] such as CdS helices [166] and hydroxyapatite (HAP) nanofibers [167].

4
Synergistic Effects of Crystal Growth Modifiers

4.1
Combination of Mixed Polymer

Usually, mineralization of $BaSO_4$ and $BaCrO_4$ minerals in the presence of poly(ethylene oxide)-*block*-poly(methacrylic acid) (PEO-*b*-PMAA) and a partially monophosphonated derivative, PEO-*b*-PMAA-PO_3H_2 (1%), can produce spherical/elongated particles and fiber bundles/cones [139, 140], respectively (Fig. 10a,b). Recently, a mixture of two DHBCs has been used to control the crystallization and organization of $BaSO_4$ microstructures as a simple model system for the synergistic action of multiple polymers in biomineralization processes [168]. The combinations of the two DHBCs at various weight ratios produced modified forms of these complex morphologies. Nucleation and outgrowth of fiber bundles/cones from spherical precursor particles could be controlled by the polymer mixing ratio to produce materials

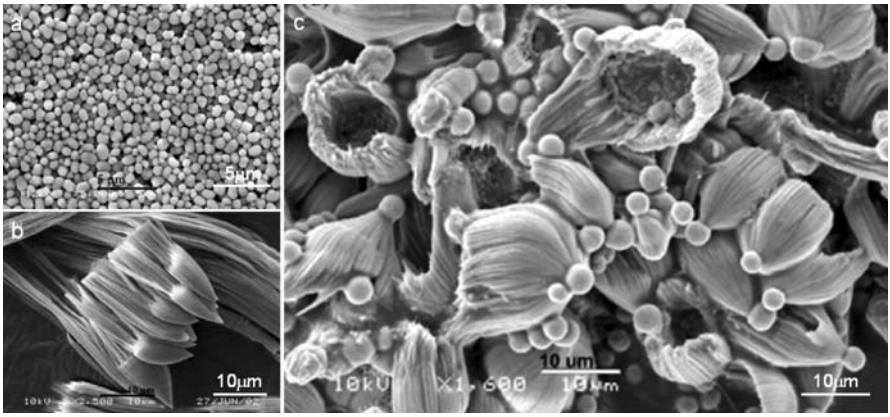

Fig. 10 $BaSO_4$ particles formed at pH 5 in the presence of **a** 1 mg mL^{-1} of PEO-*b*-PMAA, **b** 2 mg mL^{-1} of PEO-*b*-PMAA-PO_3H_2 (1%), and **c** 7 : 3 w/w mixtures of PEO-*b*-PMAA-PO_3H_2 (1%) and PEO-*b*-PMAA. (Reproduced from [168], © 2004, RSC)

with a shuttlecock-like microstructure (Fig. 10c). Disk-based cones, banded cones, or interconnecting sheets of coaligned fiber bundles can be produced at a total polymer concentration of 3 mg mL^{-1} by a cooperative mechanism involving the combined interaction of both DHBCs with growing $BaSO_4$ crystals [168]. The results reveal that the use of polymer mixtures as additives can provide new variables for crystal morphogenesis compared to systems involving an individual polymer.

4.2
Combination of Polymer with Low Mass Surfactant Molecules

The combination of polymer with low molecular mass surfactant molecules can achieve new synergistic effects on the controlled growth of inorganic crystals. Hollow structures of calcite and disklike hollow vaterite particles can be obtained by the cooperative template effects of the complex micelles formed by PEO-*b*-PMAA and sodium dodecyl sulfate (SDS) and remaining free DHBC as inhibitor in solution [169]. Similarly, the cationic surfactant cetyltrimethylammonium bromide (CTAB), which can complex the anionic PMAA groups of the DHBC, is able to induce the formation of unusual calcite pinecone-shaped particles. This concept can be further extended to synthesize hollow sub-micrometer sized Ag spheres [170]. Recently, two different soluble polymers (PEG and PMAA) were shown to cooperate with a traditional surfactant (SDS) for the synthesis of spherical calcium carbonate assemblies (e.g., hollow spheres), for which both the morphology and polymorph of the produced $CaCO_3$ crystals were controlled by varying the polymer concentration to change the corresponding transformation of the micelle structure [171].

The combination of crystallization control by DHBCs and self-organization of surfactants in an aqueous environment can lead to remarkable new crystalline structures, as also reported for similar but more simple polyelectrolyte/surfactant additives [172, 173]. Elegant featherlike $BaWO_4$ [174] and $BaMoO_4$ [175] nanostructures were prepared under mild conditions in a multistep growth mechanism by a combination of both catanionic reverse micelles (undecyl acid and decylamine) and the block copolymer PEO-*b*-PMAA itself. Numerous, nearly parallel, single crystalline barbs stand perpendicular on both sides of a polycrystalline central shaft, showing that special template effects can be achieved in a limited experimental window. These structures could be varied from starlike structures to a single shaft by simple variation of the DHBC concentration, although the role of the DHBC in the generation of these complex structures remained unclear.

4.3 Crystallization in a Mixture of Solvents

Mineralization reactions in alcohol, ethanol, isopropanol, and diethylene glycol have rarely been explored [35, 176, 177], and only $CaCO_3$ crystals with morphology such as elongated spheres or inhomogeneous aggregated structures can be obtained. In recent years, several research groups have occasionally focused on the use of different solvent media to control the crystal growth of $CaCO_3$ and other compounds [178–182]. When the crystallization conditions of $CaCO_3$ in the presence of a DHBC are modified by applying water/alcohol solvent mixtures with varying solvent compositions, and thus solvent quality changes for the block copolymer and $CaCO_3$, $CaCO_3$ nanoparticles aggregate with elongated or spherical morphologies [183].

Vaterite microspheres can be crystallized in water solution using starburst dendrimers [184] and poly(ethylene glycol)-*b*-poly(L-glutamic acid) (PEG(*m*)-*b*-pGlu(*n*)) [185] as crystal growth modifier. However, the vaterite spheres obtained are not of monodisperse feature. Recently, highly monodisperse vaterite microspheres were produced by taking advantage of the synergic effects of the block copolymer and a selectively mixed solvent under control of an artificial DHBC, PEG(*m*)-*b*-pGlu(*n*) in a mixed solvent made of a suitable volume ratio of *N*,*N*-dimethylformamide (DMF)/water (Fig. 11) [186]. This mineralization reaction in a mixed sovent may open a new general route for crystallization of minerals with high quality and structural specialty. Obviously, the property of the mixed solvent plays a key role in controlling the growth, polymorphism, and shape of the $CaCO_3$ mineral [186]. As worsening of the solvent quality for DHBCs is against the concept of well-soluble polymer additives, the mineralization in a mixed solvent can result in the formation of externally triggered DHBC aggregation, which will provide new additional experimental variables, as cation-induced micellization has shown. In addition, the mineral solubility product is sim-

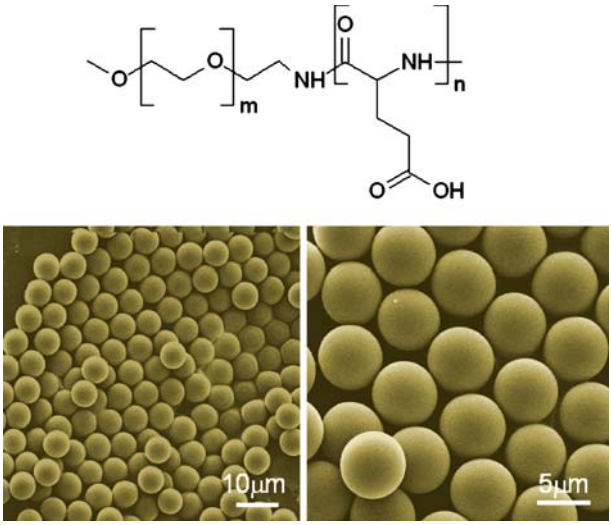

Fig. 11 *Top*: The structure of PEG (110)-*b*-pGlu(6), $m = 110$, $n = 6$. *Bottom*: Highly monodisperse vaterite $CaCO_3$ microspheres mineralized in the presence of PEG (110)-*b*-pGlu(6). The volume ratio of ethanol/water is 1 : 1.4. [PEG-*b*-pGlu] = 1 g L^{-1}; 0.6 mL $CaCl_2$ solution (0.1 M) was added to 6 mL mixed solution with different volume ratio. The crystallization reaction proceeded for 7 days at ambient temperature. (Reproduced from [186], © 2006, Wiley)

ultaneously changed in a mixed solvent system, and interesting cooperative morphogenesis scenarios may be achieved.

5
Artificial Interfaces and Matrices for Crystallization

5.1
Monolayers as Interfaces

Monolayers provide a two-dimensional matrix to mimic the biomineralization process for growing inorganic thin films or crystals [187]. The main concept behind this approach is the view pioneered by Lowenstam [188] that protein layers like, for example, the β-sheets in nacre, have an epitaxial arrangement of functional groups to specific crystal faces. The influence of surfactant headgroups with different functionalities on the crystallization of $CaCO_3$ [189–191] and $BaSO_4$ [192–194], under control of monolayers which are formed from saturated long alkyl chain carboxylates, sulfates, amines, and alcohols, has been studied.

Growth of semiconductor nanocrystals under arachidic acid (AA) monolayers by epitaxial matching of the crystals faces and the headgroups of the

surfactants leads to the formation of well-shaped nanocrystals exhibiting specific faces [195]. The PbS thin films contained uniform equilateral triangular PbS crystals, which were obtained by exposing the solution to an AA monolayer in a sealed system (Fig. 12, left). The size of the crystals can be varied by controlling the reaction time [195]. The perfect orientation growth from the $\{111\}$ basal planes can be well explained by matching the AA monolayer and the cubic PbS structures, as illustrated in Fig. 12 (right). The epitaxial growth of PbS from the $\{111\}$ face resulted from the geometrical complementarity between the monolayer and the $\{111\}$ face. The Pb – Pb and S – S interionic distances of 4.2 Å in the PbS $\{111\}$ plane geometrically matched the $d\{111\}$ spacing of 4.16 Å for the AA monolayer, as shown in Fig. 12 (right) [195]. The size and preferential orientation of PbS nanocrystals could be controlled by doping the AA monolayers with octadecylamine (ODA) [196]. Similarly, crystallization of CdS under an AA monolayer generated rodlike CdS nanostructures [197].

An interesting result that the monolayer of amphiphilic tricarboxyphenylporphyrin iron(III) μ-oxo dimers can produce highly patterned excavations resulting in "chiral" calcite crystals (Fig. 13) was demonstrated by Lahiri et al. [198]. The porphyrin presents a complex semirigid surface array of carboxylate groups intermediate between protein matrices and simple molecules. The monolayers of the μ-oxo iron(III) porphyrin dimer **1** [199] were formed at the air/water interface using a solution of **1** in 3 : 1 chloroform/methanol (1 mg/mL) to spread the film. Strikingly, about 20% of

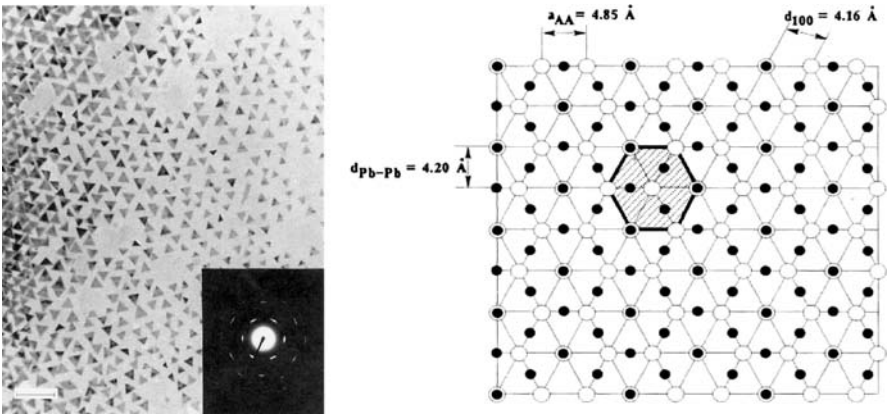

Fig. 12 *Left*: TEM image of a PbS particulate film. The *scale bar* represents 200 nm. The film was obtained by the infusion of H_2S into an arachidic acid (AA) monolayer, floating on an aqueous 5.0×10^{-4} M $Pb(NO_3)_2$ solution in a circular trough, for 45 min. The PbS film was deposited on an amorphous-carbon-coated copper grid. *Right*: Schematic diagram showing the match of the proposed overlap between Pb^{2+} ions and AA headgroups; ○ is AA headgroup and ● is Pb^{2+} ions. The *dotted line area* is a unit cell. (Reproduced from [195], © 1995, Wiley)

the three symmetry-related distal {10.4} calcite faces contained impressive rectangular cavities, and some had two or three cavities on adjoining distal {10.4} faces within which one can see clearly the layered and terraced galleries, as depicted in Fig. 13. Significantly, the crystals with a layered excavation on one {10.4} face had rectangular projections on the other, suggesting different views of the same internal structure. The results clearly show that these excavations produce an intrinsically chiral morphology even though calcite has a nonenantiomorphic crystal lattice [198]. The observed "enantiomorphs" of the crystal with chirality could only have originated from the porphyrin dimer template **1**, which must have staggered but asymmetric porphyrin planes according to molecular modeling. The molecules were found to

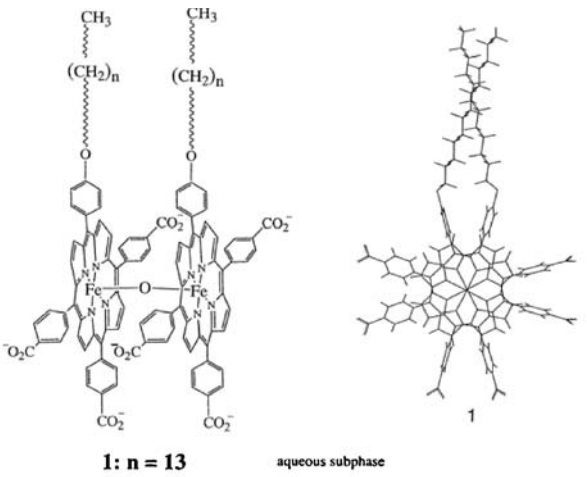

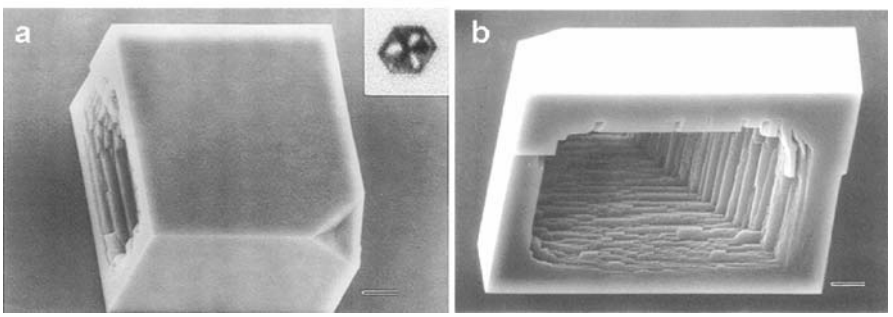

Fig. 13 *Top*: Molecular structure of the μ-oxo iron(III) porphyrin dimer. *Bottom*: SEM images of calcite crystals obtained from nucleation under **1** (**a**,**b**). **a** Image of a single calcite crystal showing the truncated corner and cavity on a distal {10.4} plane, obtained by the "dipping" method. *Inset*: An in situ optical micrograph of a calcite crystal nucleated under **1**, viewed from above. **b** View of the rectangular projections and a terraced gallery on adjoining {10.4} planes distal to the truncated corner. The *scale bar* represents 5 μm. (Reproduced from [198], © 1997, American Chemical Society)

be incorporated inside the crystal by adsorption of porphyrin from accessible surfaces, which confirmed that the highly textured laminations could be due to the anisotropic adsorption of the template **1** on specific planes of calcite crystals.

Recently, Aizenberg et al. showed an impressive example to realize face-selective nucleation of calcite on self-assembled monolayers (SAMs) of alkanethiols in which only the orientation of the functional group is varied [200]. The odd- (C_7, C_{11}, and C_{15}) and even-length (C_{10}, C_{14}, and C_{16}) carboxylic acid terminated alkylthiols supported on silver induced the nucleation of calcite from the (012) face on the basis of computer simulations on the orientation of crystals observed by SEM (Fig. 14a,b). In contrast, SAMs on gold can induced the highly oriented formation of calcite in two distinct crystallographic directions with, respectively, calcite growth from a range of (01*l*) faces ($l = 2–5$) (Fig. 14c) for the odd-length alkylthiols (C_7, C_{11}, and C_{15}), and from the (11*l*) crystallographic planes for the even chain length thiols (C_{10}, C_{14}, and C_{16}) (l = ca. 3, Fig. 14d). The results show that the variation of the orientation of the terminal groups of the molecular template could also regulate the oriented growth of crystals besides controlling the functionality and the lattice of the templating surface [200]. The lateral alignment of {012} habit-modified calcite crystals with respect to a carboxylic acid SAM of thiols on Au(111) substrate in a Kitano solution (pH 5.6–6.0) has been reported [201], implying that it is possible to precisely control the nucleation and grow other inorganic crystals with a preferred orientation to a SAM.

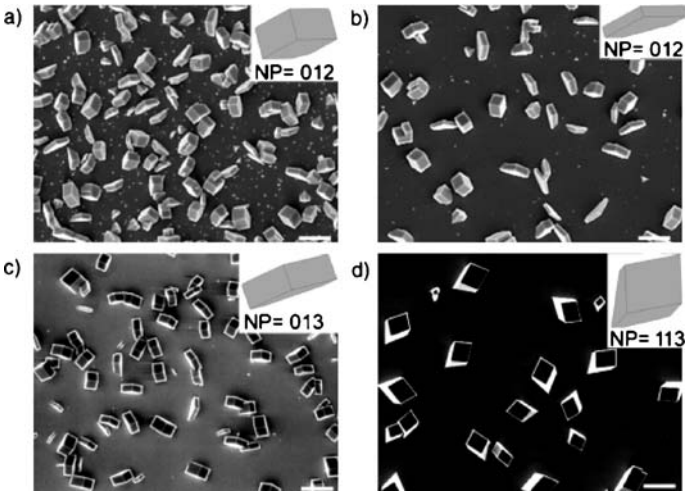

Fig. 14 SEM micrographs of calcite crystals grown on carboxylate-functionalized self-assembled monolayers of **a** C_{15} – Ag, **b** C_{10} – Ag, **c** C_{15} – Au, and **d** C_{10} – Au. The *scale bar* represents 20 μm. *Insets*: Computer simulations of similarly oriented calcite rhombohedra with the nucleating planes (NP) indicated. (Reproduced from [200], © 2003, Wiley)

In addition, crystal growth in the presence of an additive (Mg ions) can be coupled with control over the oriented nucleation achieved by using SAMs as nucleation templates [202].

5.2 Biopolymer Matrix

In Nature, there exist a few biological structures with sophisticated arrangements, such as bacterial threads [203], echinoid skeletal plates [204], eggshell membranes [205], insect wings [206], pollen grains [207], plant leaves [208], wood [209], bacterial cellulose membranes [210], filter paper, cloth, and cotton [211, 212], which were chosen as hard templates to prepare mesoporous inorganic materials with specific structures. However, heat treatment at high temperature is required to remove organic templates from the inorganic–organic hybrid materials. From the viewpoint of biomimetics, various biopolymer matrices can be chosen as templates for the synthesis of a rich family of functional materials with unusual shapes and structures. The biopolymer matrices used for material synthesis include viruses and bio-gels.

Tobacco mosaic virus (TMV) is a very stable tubelike structure of a helical RNA composed of $\sim$ 6400 bases and 2130 identical coat proteins [213, 214], which can be used as a template in the synthesis of nickel and cobalt nanowires [215], cocrystallization of CdS and PbS, iron oxides, and silica [216]. In addition, TMV particles tend to form nematic liquid crystals at a high concentration, which was used to replicate the meso nematic structure for producing mesostructured silica with periodicities of about 20 nm [217]. It is well known that peptides have limited ability of controlling composition, size, and phase during nanoparticle nucleating. Peptide of A7 and J140 has been successfully used as a hard template to prepare CdS and ZnS nanowires [218, 219], and selected M13 bacteriophage to obtain ZnS quantum dot–virus hybrid materials, single-crystal semiconductor (ZnS, CdS) [220], and magnetic (CoPt and FePt) nanowires [221].

Bio-gels are denatured protein with high molecular weight. Generally, they are hydrophilic with various functional groups and different physical and chemical properties from traditional reaction media, for example, water. The reduction of the apparent diffusion rate of the solutes in gels would decrease the nucleation and induced crystal growth through a diffusion-limited process. Theoretical studies have shown that a decrease of diffusivity can lead to a transformation process from an anisotropic shape of diffusion-limited aggregate (DLA) into an irregularly branching pattern [222]. Crystallization of fluorapatite aggregates in a gelatine gel results in the formation of a dumbbell-sphere fractal growth feature, where the intrinsic dipole electric fields may be answered for such a growth mode [223, 224]. It has been recently demonstrated that there is direct correlation between intrinsic fields caused by a parallel orientation of triple-helical protein fibers of gelatine and

the self-organized growth of the biocomposite system fluorapatite–gelatine based on an electron holography imaging technique [225].

It is noted that the surface of the sphere is composed of closely packed needlelike units; this kind of crystal is called a "mesocrystal" [226]. Mesocrystals often had a higher symmetry than their constituent tectons [226]. The reactions in gels which are expected to generate mesocrystals need very high supersaturation, leading to increased nucleation number of small clusters as building units for assembly to mesocrystals [227]. Porous hexagonal prism single-crystalline $CaCO_3$ crystals were obtained via self-oriented attachment of the nanocrystals from a reaction between urea and calcium nitrate in a lime-cured gelatine system [228].

Imai and coworkers extended the research of crystal growth in gel media. Their results [229, 230] indicated that in agar, gelatine, and pectin gels, crystals of triclinic systems (H_3BO_3 and $K_2Cr_2O_7$) tended to form peculiar curved and helical branches because of the lowest symmetry of subunits in the polycrystalline material. In the diffusion field (gel system), the connected joints of twinned crystals in aggregates deviated from each other. Unique DLA-like morphologies including twisted branches can be obtained at a band of further increase in gel density, while cubic crystals (NH_4Cl and $Ba(NO_3)_2$) were never found in twisted form under any conditions.

Regular surface-relief calcium carbonate structures were prepared by a cooperated directing agent of soluble poly(acrylic acid) (PAA, $M_w = 2000$) and a substrate of cholesterol-bearing pullulans (Fig. 15) [231]. At low temperature, adapted PAA concentration, and with cholesteryl groups, a high quality periodic calcite structure can be formed by a self-organization process in the reaction–diffusion system with competition between precipitation and ion diffusion.

A predesigned, self-assembled organogelator as template, which resembles the organic matrix in biomineralization used by organic systems to transcribe

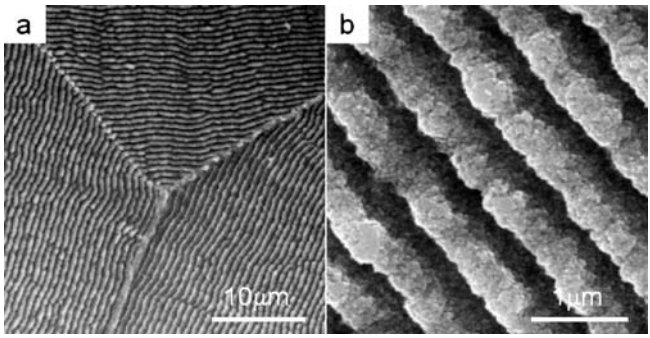

Fig. 15 SEM images of patterned $CaCO_3$ crystals grown on CHP-3 matrices, 20°, 2 days, [PAA] = 2.4×10^{-3} wt %. **a** A boundary among patterned films; **b** a magnified image. (Reproduced from [231], © 2003, Wiley)

inorganic nanostructures, has been intensively studied [18]. A recent paper first reported the synthesis of the nacre morphology by a remineralization process with the introduction of poly(aspartic acid) on the insoluble organic matrix of *Haliotis laevigata*, as for mineralization in Nature [232].

5.3 Synthetic Polymer Matrix

Imai and coworkers [229, 230] also investigated the crystal growth of the triclinic system (H_3BO_3 and $K_2Cr_2O_7$) and cubic crystals (NH_4Cl and $Ba(NO_3)_2$) in synthetic gels, for example, poly(vinyl alcohol) (PVA, M_w = 22 000) and poly(acrylic acid) (PAA, M_w = 250 000, 35 wt % aqueous solution). They obtained similar results to those that occurred in bio-gels, except there existed almost the same amounts of left- and right-handed helices in PAA and PVA matrices, whereas right-handed helices dominated in the bio-gels such as agar, gelatine, and pectin (Fig. 16). Precise control of the chirality of $K_2Cr_2O_7$ crystals in PAA gel [233] can be achieved by addition of a specified amount of chiral molecules (D- and L-glutamic) which can selectively adsorbed on (010) and ($0\bar{1}0$) faces of $K_2Cr_2O_7$. For a crystal with a relatively high symmetry, orthorhombic K_2SO_4 can also form a helical morphology at a high concentration of PAA under control of a DLA process [234].

Potassium sulfate and potassium hydrogen phthalate both formed a nacre-like structure when the PAA concentration was adjusted to a suitable value [235–237] (Fig. 17). Just like the nacre in Nature (Japanese pearl oyster: *Pinctada fucata*) [235], the nacre-like structure of potassium sulfate–PAA and potassium hydrogen phthalate–PAA can absorb and store dyes [235–237] (Fig. 17). With a different concentration of PAA, the K_2SO_4 crystal exhibited a different hierarchical architecture by "iso-oriented assembly" or "oriented attachment" mechanisms [236].

There also existed another use of synthetic polymers besides synthetic gels as the hard template to influence crystal growth discussed above. In this case, solid synthetic polymers were used as a "real hard template". It has been demonstrated that calcium carbonate favored the formation of the vaterite phase on the poly(vinyl chloride-*co*-vinyl acetate-*co*-maleic acid) substrate in the supersaturated solution prepared from calcium nitrate and sodium dicarbonate solutions at pH 8.50 [238]. Commercial polymer fiber (Nylon 66 and Kevlar 29) can induce crystallization of calcite in solution, but the vaterite phase tends to crystallize on the surface of polymers in the presence of soluble polymer (PVA), and aragonite favors forming on the surface of polymers modified with acid or alkali accompanying PVA [239].

Recently, a new type of synthetic polymer which consists of condensed particles (hard part) and polymeric functional blocks (soft part) has been used for the mineralization of calcium carbonate [240, 241]. Poly(diethylaminoethyl methacrylate)-*b*-poly(*N*-isopropyl acrylamide)-*b*-poly(metha-

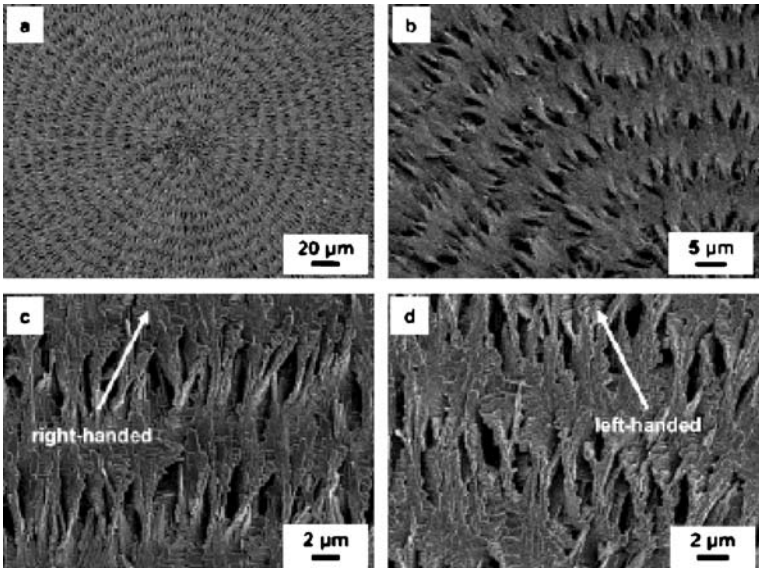

Fig. 16 Typical field-emission SEM (FESEM) images of the $K_2Cr_2O_7$ helical architectures grown in PAA gel matrix without additives after evaporation of water. **a** Spherulitic morphology. **b** Branches having a helical architecture in the spherulite. **c,d** Right- and left-handed helical forms, respectively. (Reproduced from [233], © 2004, American Chemical Society)

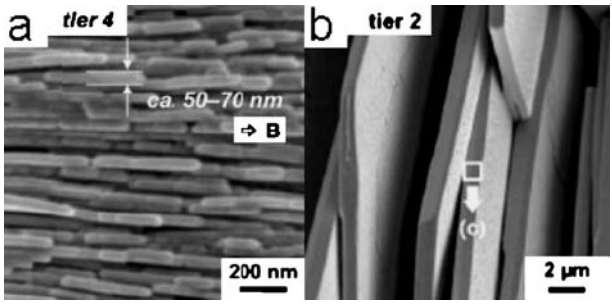

Fig. 17 Typical FESEM images. **a** K_2SO_4 in PAA gel, $C_{PAA} = 8\,g\,dm^{-3}$. (Reproduced with permission from [236], © 2005, Wiley). **b** Potassium hydrogen phthalate in PAA gel, $C_{PAA} = 10–15\,g\,dm^{-3}$. (Reproduced from [237], © 2005, RSC)

crylic acid) (PDEAEMA-*b*-PNIPAM-*b*-PMAA; hydrodynamic diameter of the particle in water is about 1 µm), which has both an outer positive (PDEAEMA) and an inner negative (PMAA) block, while the PNIPAM block is regarded as mediating sufficient steric stability, is successfully used to produce stable "sheaf bundle" aragonite with a 1-µm hole in the bottom of the structure (Fig. 18a,b) [240]. A porous single calcite crystal was synthesized

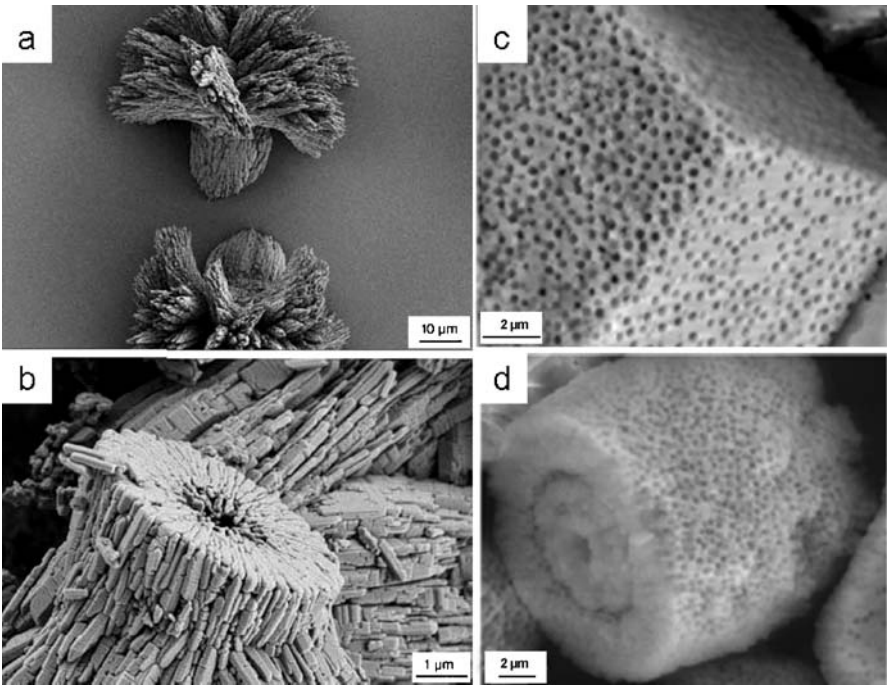

Fig. 18 Typical FESEM images of **a**,**b** "sheaf bundle" aragonite (reproduced from [240], © 2005, Wiley), and **c**,**d** porous single calcite (reproduced from [241], © 2004, American Chemical Society)

by poly(styrene(St)-*b*-methyl methacrylate (MMA)-*b*-acrylic acid (AA)) with different diameters (Fig. 18c,d) [241]. Crystal growth in the presence of this type of polymer showed remarkably different effects from other polymers and deserves further investigation.

5.4 Crystallization on Foreign External Templates

From the above examples, it is clear that DHBCs themselves can promote the formation of complex crystal morphologies, often involving nanoscopic building units. It is interesting to investigate the influence of an external template on a DHBC-controlled crystallization system. These foreign external templates include CO_2 or air bubbles, charged particles, and air/water interfaces.

In one reported example, the chosen template was as simple as CO_2 bubbles, which are generated by CO_2 evaporation from supersaturated $Ca(HCO_3)_2$ solutions (Kitano method). The gas bubbles were used to act as a foreign external template to produce $CaCO_3$ particles with complex mor-

phologies [134, 137]. Similarly, a combination of the mineralization under control of low molecular weight polyelectrolytes and a foreign static template such as air bubbles has been explored for the generation of macroporous $BaCO_3$ spherulites [93], which is similar to that found in the microemulsion system reported by Mann et al. [242].

Furthermore, charged particles can also be used as templates instead of gas bubbles to break the previous constraint of bundle formation in $BaSO_4$/$BaCrO_4$ crystallization controlled by a phosphonated DHBC [95, 101]. Separated $BaCrO_4$ single crystalline nanofibers with extremely high aspect ratios of > 5000 can be produced through a combination of crystal growth control by DHBCs and controlled nucleation provided by cationic colloidal particles [143].

It has been proved that the basic polymers, which will be positively charged under acidic conditions, are also useful templates for the growth of calcium carbonate [243]. Hemispherical vaterite and needlelike aragonite can be selectively synthesized at the air/water interface by the mediation of poly(ethylene imines)(PEIs) dissolved in supersaturated calcium bicarbonate solution with different molecular weight of PEI blocks, suggesting that cationic polychains are also versatile templates for artificial material synthesis.

Recently, the influence of poly(ethylene glycol)-*block*-poly(ethylene imine) (PEG-*b*-PEI-linear), which is a family of cationic DHBCs, on the crystallization of calcium carbonate at the air/water interface has been studied [244]. The results demonstrated that the crystal morphology of calcium carbonate with layered structures formed at the air/water surface can be well controlled with different PEI block lengths and pH values of the initial solution. The results demonstrated that either PEI length or the solution acidity has significant influence on the morphogenesis of vaterite crystals at the air/water interface (Fig. 19). A possible mechanism for the stratification of $CaCO_3$ vaterite crystals has been proposed. Increasing either PEI length or the initial pH value of the solution will decrease the density of the PEG block anchored

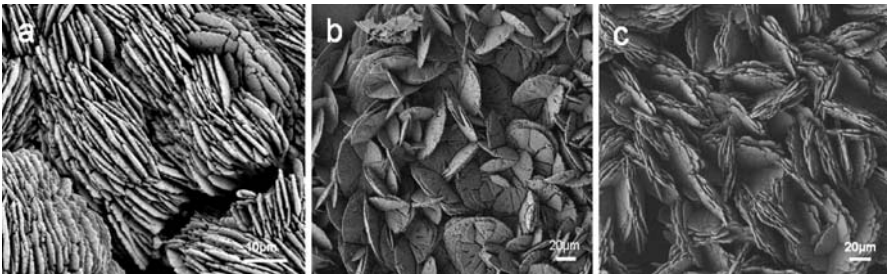

Fig. 19 SEM images of $CaCO_3$ superstructures formed at an air/water interface in the presence of PEG_{5000}-*b*-PEI_{1200}; the initial pH value is 4. **a** PEG_{5000}-*b*-PEI_{1200}, 2 g L^{-1}; **b**, **c** PEG_{5000}-*b*-PEI_{400}; the initial pH values are 4 and 3, respectively. The mineralization time is 5 days. (Reproduced from [244], © 2006, American Chemical Society)

on the binding interface and result in exposing more space as binding interface to solution and favoring the subnucleation and stratification growth on the polymer/$CaCO_3$ interface. In contrast, a higher density of PEG blocks will stabilize the growing crystals more efficiently and inhibit subnucleation on the polymer/$CaCO_3$ interface, thus preventing the formation of stratified structures. This study provides an example which shows that it is possible to access the morphogenesis of calcium carbonate structures by the combination of a block copolymer with an air/water interface.

The above results emphasized that the foreign external templates can be combined with a polymer or polyelectrolyte and provide an additional tool for controlled morphogenesis of inorganic minerals.

5.5 Crystallization on Patterned Surfaces

Crystallization on the monolayer interface and on external templates has been intensively explored in the past few decades (Sects. 5.1 and 5.4). Emerging trends in the field of surface induced crystallization have been focused on how to precisely control the crystallization events, the density and pattern of nucleation events, and the sizes and orientations of the growing crystals. Micropatterned self-assembled monolayers afford control over all these parameters as demonstrated in the crystallization of inorganic crystals [245] and organic crystals [246]. Aizenberg reviewed the bio-inspired approaches to artificial crystallization based on the principles of biomineralization occurring within specific microenvironments [17]. Tailoring of self-assembled monolayers (SAMs) based on modern soft lithography techniques can provide well-defined patterned surfaces for the nucleation of calcium carbonate. Crystallization on these patterned surfaces can result in the formation of large-area, high-resolution inorganic replicas of the underlying organic patterns with advantages including controlled localization of particles, nucleation density, crystal sizes, crystallographic orientation, morphology, polymorphism, stability, and architecture [17, 245, 247].

Biological systems provide numerous examples of micropatterned inorganic materials that directly develop into their intricate architectures, as illustrated by skeleton formation in echinoderms with component function of specialized photosensory organs [19, 248]. Each skeletal structural unit (spines, test plates) is composed of a single calcite crystal delicately patterned on the micrometer scale, which is composed of a close-set array of hemispherical calcitic structures (40–50 μm in diameter) with a characteristic double-lens design (Fig. 20).

In order to mimic such biological structure found in echinoderms, Aizenberg et al. developed a bio-inspired approach to growing large micropatterned calcitic single crystals with controlled orientation and microstructure by crystallization on well-designed micropatterned substrates [247], repre-

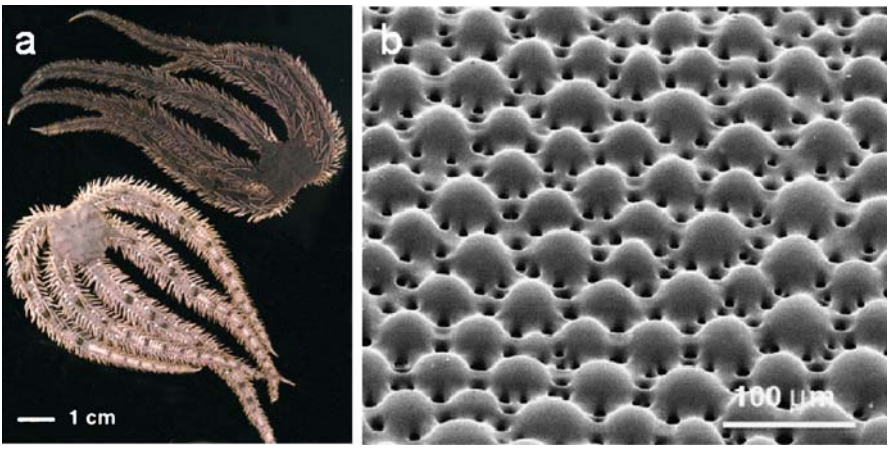

Fig. 20 **a** The same individual of the brittlestar *Ophiocoma Wendtii*, photographed during the day (*top*) and during the night (*bottom*). **b** SEM image of an array of microlenses on the surface of the dorsal arm plate in *O. Wendtii*. (Reproduced from [248], © 2004, RSC)

senting a general strategy for the design of micro- and nanopatterned crystalline materials (Fig. 21a). In this approach, micropatterned templates, which were organically modified to induce the formation of metastable amorphous calcium carbonate, were nicely imprinted with calcite nucleation sites, resulting in successful template-directed deposition and crystallization of the

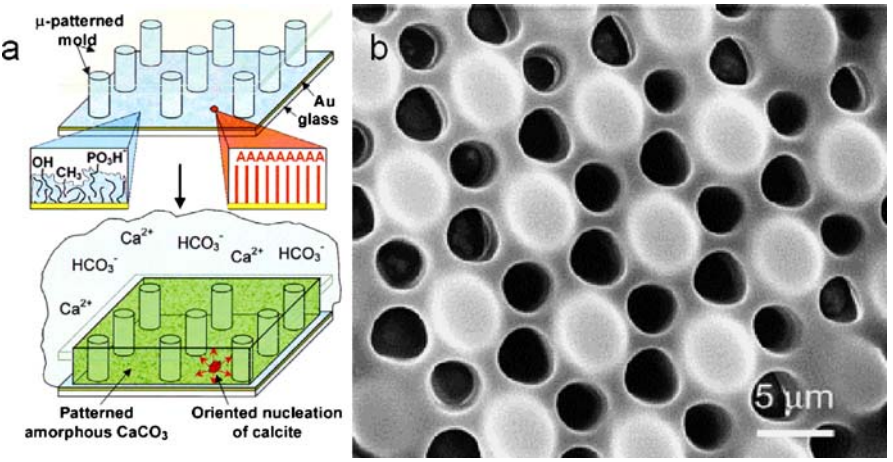

Fig. 21 **a** Schematic illustration of the new approach for the formation of "microperforated" single crystals: deposition of the ACC mesh from the $CaCO_3$ solution, oriented nucleation at the imprinted nucleation site, and the amorphous-to-crystalline transition of the ACC film on the engineered 3D templates. (Reproduced from [247], © 2003, American Association for the Advancement of Science)

amorphous phase into millimeter-sized single calcite crystals with sub-10-μm patterns and controlled crystallographic orientation (Fig. 21b), which quite resembles the natural skeleton in echinoderms (Fig. 20b). The results indicated that the predesigned three-dimensional templates not only stabilize the ACC and control the oriented crystal nucleation and the micropattern of single crystals, but also act as stress release sites and discharge sumps for excess water and impurities during crystallization [246]. Recently, three-beam interference lithography was used to create a synthetic, biomimetic analog of the brittlestar microlens array with integrated lenses and pores [249].

Such biomimetic synthetic microlens arrays could be potentially used as highly tunable optical elements for a wide variety of applications [246, 247, 249]. The successful fabrication of micropatterned single crystals resembling the natural echinoderm calcitic structures demonstrated that the inspiration from Nature's methods of biological manufacture is proving to be a rich reservoir for the fabrication of advanced materials and devices with novel and superior properties.

6 Summary and Outlook

In summary, recent progress on bio-inspired crystal growth by synthetic templates has been overviewed. Soluble polymer soft templates such as biopolymers and synthetic polymers have shown remarkable effects on the directed crystal growth and controlled self-assembly of inorganic nanoparticles. Different morphogenesis mechanisms of crystal growth such as selective adsorption, mesoscopic transformations, and higher order assembly have been discussed. Recent new developments demonstrated that these soluble polymer soft templates can be combined with other low mass organic molecules or be used in a mixed solvent system to achieve flexible synergistic effects on the mineralization and controlled growth of inorganic crystals with complex form. In contrast, insoluble polymers with different functionalities can be used as a hard template or substrates that offer suitable crystallization sites for the guided crystallization and self-assembly processes. Crystallization on artificial interfaces including monolayers, biopolymer and synthetic polymer matrices for controlled crystal growth, and emerging crystallization on patterned surfaces for the creation of patterned crystals provide additional means to control morphology, microstructure, complexity, and length scales of various inorganic nanostructured materials with two and three dimensionalities.

Recent advances have demonstrated that synthetic template directed crystal growth and mediated self-assembly of nanoparticles can provide promising ways for the rational design of various ordered inorganic and inorganic–organic hybrid materials with complexity and structural specialty. However,

there is still a lack of understanding of the nucleation, crystallization, self-assembly, and growth mechanisms of complex superstructures in solution systems. Further multidisciplinary efforts are needed to overcome analytical difficulties which are associated with investigating a multistep and multicomponent morphogenesis mechanism in solution systems. Especially, the detailed interactions on the "soft/hard" interfaces (organic/inorganic interfaces) have to be studied systematically with the help of multianalytical techniques to reveal the real mechanism for the formation of complex matter in solution.

Further exploration in these areas should open new avenues for rationally designing various kinds of inorganic and inorganic–organic hybrid materials with ideal hierarchy at controllable length scales, and desirable dimensionality by bio-inspired approaches. In addition, the study of the relationship between the structural specialty/complexity (shape, size, phase, dimensionality, hierarchy etc.) of the synthetic materials by bio-inspired approaches and their properties will shed new light on the potential but important applications of these materials in various fields in the future.

Acknowledgements S.-H. Yu thanks for the special funding support by the Century Program of the Chinese Academy of Sciences, and the Natural Science Foundation of China (NSFC, Contract Nos. 20325104, 20321101, and 50372065), the Scientific Research Foundation for the Returned Overseas Chinese Scholars supported by the State Education Ministry, the Specialized Research Fund for the Doctoral Program (SRFDP) of Higher Education State Education Ministry, and the Partner Group of the Chinese Academy of Sciences—the Max Planck Society.

References

1. Mann S (1997) In: Bruce DW, O'Hare D (eds) Inorganic materials. Wiley, New York, pp 256–311
2. Mann S, Webb J, Williams RJP (1989) Biomineralization. Wiley, Weinheim
3. Mann S, Ozin GA (1996) Nature 382:313
4. Mann S (2000) Angew Chem Int Ed 39:3393
5. Dujardin E, Mann S (2002) Adv Mater 14:775
6. Estroff LA, Hamilton AD (2001) Chem Mater 13:3227
7. Ozin GA (1997) Acc Chem Res 30:17
8. Ozin GA (2000) Chem Commun 419
9. Kato T, Sugawara A, Hosoda N (2002) Adv Mater 14:869
10. Cölfen H, Mann S (2003) Angew Chem Int Ed 42:2350
11. Mann S (ed) (1996) Biomimetic materials chemistry. Wiley, New York
12. Davis SA, Breulmann M, Rhodes KH, Zhang B, Mann S (2001) Chem Mater 13:3218
13. Antonietti M (2003) Nat Mater 2:9
14. Weiner SW, Addadi L (1997) J Mater Chem 7:689
15. Dabbs DM, Aksay A (2000) Annu Rev Phys Chem 51:601
16. Mann S (1997) J Chem Soc Dalton Trans 3953
17. Aizenberg J (2004) Adv Mater 16:1295
18. Aizenberg J, Hendler G (2004) J Am Chem Soc 126:9271

19. Aizenberg J, Tkachenko A, Weiner S, Addadi L, Hendler G (2001) Nature 412:819
20. van Bommel KJC, Friggeri A, Shinkai S (2003) Angew Chem Int Ed 42:980
21. Matijević E (1993) Chem Mater 5:412
22. Matijević E (1996) Curr Opin Colloid Interface Sci 1:176
23. Antonietti M, Göltner C (1997) Angew Chem Int Ed 36:910
24. Archibald DD, Mann S (1993) Nature 364:430
25. Yang H, Coombs N, Ozin GA (1997) Nature 386:692
26. Li M, Schnablegger H, Mann S (1999) Nature 402:393
27. Peng XG, Manna L, Yang WD, Wickham J, Scher E, Kadavanich A, Alivisatos AP (2000) Nature 404:59
28. Ahmadi TS, Wang ZL, Green TC, Henglein A, El-Sayed MA (1996) Science 272:1924
29. Gibson CP, Putzer K (1995) Science 267:1338
30. Pileni MP, Ninham BW, Gulik-Krzywicki T, Tanori J, Lisiecki I, Filankembo A (1999) Adv Mater 11:1358
31. Park SJ, Kim S, Lee S, Khim ZG, Char K, Hyeon T (2000) J Am Chem Soc 122:8581
32. Adair JH, Suvaci E (2001) Curr Opin Colloid Interface Sci 5:160
33. Bäuerlein E (2003) Angew Chem Int Ed 42:614
34. Niemeyer CM (2001) Angew Chem Int Ed 40:4128
35. Cölfen H (2001) Macromol Rapid Commun 22:219
36. Yu SH, Cölfen H (2004) J Mater Chem 14:2124
37. Cölfen H, Yu SH (2005) MRS Bull 30:727
38. Yu SH, Chen SF (2006) Curr Nanosci 2:81
39. Wulff G (1901) Z. Krystallogr 34:449
40. Buckley HE (1951) Crystal growth. Wiley, New York
41. Mullin IJW (1971) Crystallization. Butterworths, London
42. Chernov AA (1974) J Cryst Growth 24/25:11
43. Kudora T, Irisawa T, Ookawa A (1977) J Cryst Growth 42:41
44. Berg WF (1938) Proc R Soc London Ser A 164:79
45. Bunn CW (1949) Discuss Faraday Soc 5:132
46. Siegfried MJ, Choi KS (2005) Angew Chem Int Ed 44:3218
47. Siegfried MJ, Choi KS (2004) Adv Mater 16:1743
48. Penn RL, Banfield JF (1999) Geochim Cosmochim Acta 63:1549
49. Penn RL, Oskam G, Strathmann TJ, Searson PC, Stone AT, Veblen DR (2001) J Phys Chem B 105:2177
50. Penn RL, Stone AT, Veblen DR (2001) J Phys Chem B 105:4690
51. Penn RL, Banfield JF (1998) Science 281:969
52. Banfield F, Welch SA, Zhang H, Ebert TT, Penn RL (2000) Science 289:751
53. Cölfen H, Antonietti M (2005) Angew Chem Int Ed 44:5576
54. Yu SH (2005) Biomineralized inorganic materials. In: Nalwa HS (ed) Handbook of nanostructured biomaterials and their applications, vol 1. American Scientific, Los Angeles, pp 1–69
55. Antonietti M (2001) Curr Opin Colloid Interface Sci 6:244
56. Hardikar VV, Matijević E (2001) Colloids Surf A 186:23
57. Shen FH, Feng QL, Wang CM (2002) J Cryst Growth 242:239
58. Belcheer AM, Wu HX, Christensen RJ, Hansma PK, Stucky GD, Morse DE (1996) Nature 381:56
59. Feng QL, Pu G, Pei Y, Cui FZ, Li HD, Kim TN (2000) J Cryst Growth 216:459
60. Raz S, Weiner S, Addadi L (2000) Adv Mater 12:38
61. Belcher AM, Wu XH, Christensen RJ, Hansma PK, Stucky GD, Morse DE (1996) Nature 381:56

62. Falini G, Albeck S, Weiner S, Addadi L (1996) Science 271:67
63. DeOliveira DB, Laursen RA (1997) J Am Chem Soc 119:10627
64. Li CM, Botsaris GD, Kaplan DL (2002) Cryst Growth Des 2:387
65. Arias JL, Fernandez MS (2003) Mater Charact 50:189
66. Mirkin CA (2000) Inorg Chem 39:2258
67. Mirkin CA, Letsinger RL, Mucic RC, Storhoff JJ (1996) Nature 382:607
68. Alivisatos AP, Johnson K, Peng X, Wilson TE, Loweth CJ, Bruchez M, Schultz PG (1996) Nature 382:609
69. Dujardin E, Hsin LB, Wang CRC, Mann S (2001) Chem Commun 1264
70. Lee SW, Lee SK, Belcher AM (2003) Adv Mater 15:689
71. Dujardin E, Peet C, Stubbs G, Culver JN, Mann S (2003) Nano Lett 3:413
72. Mao C, Flynn CE, Hayhurst A, Sweeney R, Qi J, Georgiou G, Iverson B, Belcher AM (2003) Proc Natl Acad Sci USA 100:6946
73. Vali H, Weiss B, Li YL, Sears SK, Kim SS, Kirschvink JL, Zhang CL (2004) Proc Natl Acad Sci USA 101:16121
74. Bharde A, Wani A, Shouche Y, Joy PA, Prasad BLV, Sastry M (2005) J Am Chem Soc 127:9326
75. Mann S, Sparks NHC, Frankel RB, Bazylinskida DA, Jannasch HW (1990) Nature 343:258
76. Rautaray D, Ahmad A, Sastry M (2003) J Am Chem Soc 125:14656
77. Rautaray D, Ahmad A, Sastry M (2004) J Mater Chem 14:2333
78. Rautaray D, Sanyal A, Adyanthaya SD, Ahmad A, Sastry M (2004) Langmuir 20:6827
79. Ahmad A, Rautaray D, Sastry M (2004) Adv Funct Mater 14:1075
80. Shankar SS, Rai A, Ankamwar B, Singh A, Ahmad A, Sastry M (2004) Nat Mater 3:482
81. Shankar SS, Rai A, Ahmad A, Sastry M (2004) J Colloid Interface Sci 275:496
82. Kröger N, Deutzmann R, Sumper M (1996) Science 286:1129
83. Kröger N, Deutzmann R, Bergsdorf C, Sumper M (2000) Proc Natl Acad Sci USA 97:14133
84. Kröger N, Lorenz S, Brunner E, Sumper M (2002) Science 298:584
85. Sumper M (2002) Science 295:2430
86. Menzel H, Horstmann S, Behrens P, Bärnreuther P, Krueger I, Jahns M (2003) Chem Commun 2994
87. Cha JN, Stucky GD, Morse DE (2000) Nature 403:289
88. Cha JN, Shimizu K, Zhou Y, Christiansen SC, Chmelka BF, Stucky GD, Morse DE (1996) Proc Natl Acad Sci USA 96:361
89. Rieger J (2002) Tenside Surfactants Deterg 39:221
90. Peytcheva A, Cölfen H, Antonietti M (2002) Colloid Polym Sci 280:218
91. Gower LB, Tirrell DA (1998) J Cryst Growth 191:153
92. Gower LB, Odom DJ (2000) J Cryst Growth 210:719
93. Yu SH, Cölfen H, Xu AW, Dong WF (2004) Cryst Growth Des 4:33
94. Bigi A, Boanini E, Walsh D, Mann S (2002) Angew Chem Int Ed 41:2163
95. Qi LM, Cölfen H, Antonietti M, Li M, Hopwood JD, Ashley AJ, Mann S (2001) Chem Eur J 7:3526
96. Yu SH, Antonietti M, Cölfen H, Hartmann J (2003) Nano Lett 3:379
97. Olszta MJ, Odom DJ, Douglas EP, Gower LB (2003) Connect Tissue Res 44 (Suppl. 1):326
98. Olszta MJ, Gajjeraman S, Kaufman M, Gower LB (2004) Chem Mater 16:2355
99. Wagner RS, Ellis WC (1964) Appl Phys Lett 4:89
100. Trentler TJ, Hickman KM, Goel SC, Viano AM, Gibbons PC, Buhro WE (1995) Science 270:1791

101. Yu SH, Cölfen H, Antonietti M (2002) Chem Eur J 8:2937
102. Jada J, Verraes A (2003) Colloids Surf A 219:7
103. Shchukin DG, Sukhorukov GB, Mohwald H (2003) Chem Mater 15:3947
104. Wang TX, Cölfen H, Antonietti M (2005) J Am Chem Soc 127:3246
105. Donners JJJM, Nolte RJM, Sommerdijk NAJM (2002) J Am Chem Soc 124:9700
106. Ueyama N, Hosoi T, Yamada Y, Doi M, Okamura T, Nakamura A (1998) Macromolecules 31:7119
107. Ueyama N, Kozuki H, Doi M, Yamada Y, Takahashi K, Onoda A, Okamura T, Yamamoto H (2001) Macromolecules 34:2607
108. Ueyama N, Takeda J, Yamada Y, Onoda A, Okamura T, Nakamura A (1998) Inorg Chem 38:475
109. Sugawara T, Suwa Y, Ohkawa K, Yamamoto Y (2003) Macromol Rapid Commun 24:847
110. Zhang ZP, Gao D, Zhao H, Xie C, Guan G, Wang D, Yu SH (2006) J Phys Chem B 110:8613
111. Xu AW, Antonietti M, Cölfen H, Fang YP (2006) Adv Funct Mater 16:903
112. Xu AW, Yu Q, Dong WF, Antonietti M, Cölfen H (2005) Adv Mater 17:2217
113. Peng Y, Xu AW, Deng B, Antonietti M, Cölfen H (2006) J Phys Chem B 110:2988
114. Kotachi A, Miura T, Imai H (2004) Chem Mater 16:3191
115. Wegner G, Baum P, Müller M, Norwig J, Landfester K (2001) Macromol Symp 175:349
116. Basko M, Kubisa P (2002) Macromolecules 35:8948
117. Basko M, Kubisa P (2004) J Polym Sci A Polym Chem 42:1189
118. Förster S, Plantenberg T (2002) Angew Chem Int Ed 41:689
119. Kriesel JW, Sander MS, Tilley TD (2001) Chem Mater 13:3554
120. Bronstein LM, Sidorov SN, Gourkova AY, Valetsky PM, Hartmann J, Breulmann M, Cölfen H, Antonietti M (1998) Inorg Chim Acta 280:348
121. Sidorov SN, Bronstein LM, Valetsky PM, Hartmann J, Cölfen H, Schnablegger H, Antonietti M (1999) J Colloid Interface Sci 212:197
122. Bronstein LM, Sidorov SN, Valetsky PM, Hartmann J, Cölfen H, Antonietti M (1999) Langmuir 15:6256
123. Yu SH, Cölfen H, Mastai Y (2004) J Nanosci Nanotechnol 4:291
124. Zhang D, Qi LM, Ma JM, Cheng HM (2001) Chem Mater 13:2753
125. Qi LM, Cölfen H, Antonietti M (2002) Nano Lett 1:61
126. Bouyer F, Gérardin C, Fajula F, Putaux JL, Chopin T (2003) Colloids Surf A 217:179
127. Sedlak M, Antonietti M, Cölfen H (1998) Macromol Chem Phys 199:247
128. Sedlak M, Cölfen H (2001) Macromol Chem Phys 202:587
129. Cölfen H, Antonietti M (1998) Langmuir 14:582
130. Cölfen H, Qi LM (2001) Chem Eur J 7:106
131. Marentette JM, Norwig J, Stockelmann E, Meyer WH, Wegner G (1997) Adv Mater 9:647
132. Norwig J (1997) Mol Cryst Liq Cryst 313:115
133. Yu SH, Cölfen H, Hartmann J, Antonietti M (2002) Adv Funct Mater 12:541
134. Rudloff J, Antonietti M, Cölfen H, Pretula J, Kaluzynski K, Penczek S (2002) Macromol Chem Phys 203:627
135. Kaluzynski K, Pretula J, Lapienis G, Basko M, Bartczak Z, Dworak A, Penczek S (2001) J Polym Sci A Polym Chem 39:955
136. Yu S-H, Cölfen H, Antonietti M (2003) J Phys Chem B 107:7396
137. Rudloff J, Cölfen H (2004) Langmuir 20:991
138. Antonietti M, Breulmann M, Göltner C, Cölfen H, Wong KK, Walsh D, Mann S (1998) Chem Eur J 4:2493

139. Qi LM, Cölfen H, Antonietti M (2000) Angew Chem Int Ed 39:604
140. Qi LM, Cölfen H, Antonietti M (2002) Chem Mater 12:2392
141. Cölfen H, Qi LM, Mastai Y, Börger L (2002) Cryst Growth Des 2:191
142. Robinson KL, Weaver JVM, Armes SP, Marti ED, Meldrum FC (2002) J Mater Chem 12:890
143. Yu S-H, Cölfen H, Antonietti M (2003) Adv Mater 15:133
144. Bagwell RB, Sindel J, Sigmund W (1999) J Mater Res 14:1844
145. Zhang DB, Qi LM, Ma JM, Cheng HM (2002) Chem Mater 14:2450
146. Öner M, Norwig J, Meyer WH, Wegner G (1998) Chem Mater 10:460
147. Taubert A, Palms D, Weiss O, Piccini MT, Batchelder DN (2002) Chem Mater 14:2594
148. Taubert A, Palms D, Glasser G (2002) Langmuir 18:4488
149. Taubert A, Kübel C, Martin DC (2003) J Phys Chem B 107:2660
150. Yu SH, Antonietti M, Cölfen H, Giersig M (2002) Angew Chem Int Ed 41:2356
151. Mastai Y, Sedlák M, Cölfen H, Antonietti M (2002) Chem Eur J 8:2430
152. Qi LM (2001) J Mater Sci Lett 20:2153
153. Mastai Y, Rudloff J, Cölfen H, Antonietti M (2002) ChemPhysChem 3:119
154. Chen SF, Yu SH, Wang TX, Jiang J, Cölfen H, Hu B, Yu B (2005) Adv Mater 17:1461
155. Cölfen H (2001) Macromol Rapid Commun 22:219
156. Gao YX, Yu SH, Cong H, Jiang J, Xu AW, Dong WF, Cölfen H (2006) J Phys Chem B 110:6432
157. Yu SH, Cölfen H, Tauer K, Antonietti M (2005) Nat Mater 5:51
158. Wang TX, Xu AW, Cölfen H (2006) Angew Chem Int Ed 45:4451
159. Naka K (2003) Top Curr Chem 228:141
160. Naka K, Tanaka Y, Chujo Y, Ito Y (1999) Chem Commun 1931
161. Naka K, Tanaka Y, Chujo Y (2002) Langmuir 18:3655
162. Donners JJJM, Heywood BR, Meijer WM, Nolte RJM, Roman C, Schenning APLHJ, Sommerdijk NAJM (2000) Chem Commun 1937
163. Donners JJJM, Heywood BR, Meijer WM, Nolte RJM, Sommerdijk NAJM (2002) Chem Eur J 8:2561
164. Estroff LA, Incarvito CD, Hamilton AD (2004) J Am Chem Soc 126:2
165. Hartgerink JD, Zubarev ER, Stupp SI (2001) Curr Opin Colloid Interface Sci 5:355
166. Sone ED, Zubarev ER, Stupp SI (2002) Angew Chem Int Ed 41:1705
167. Hartgerink JD, Beniash E, Stupp SI (2001) Science 294:1684
168. Li M, Mann S, Cölfen H (2004) J Mater Chem 14:2269
169. Qi LM, Li J, Ma JM (2000) Adv Mater 14:300
170. Zhang D, Qi LM, Ma JM, Cheng HM (2002) Adv Mater 14:1499
171. Deng SG, Cao JM, Feng J, Guo J, Fang BQ, Zheng MB, Tao J (2005) J Phys Chem B 109:11473
172. Wei H, Shen Q, Zhao Y, Wang D, Xu D (2004) J Cryst Growth 260:511
173. Wei H, Shen Q, Zhao Y, Wang D, Xu D (2004) J Cryst Growth 260:545
174. Shi HT, Qi LM, Ma JM, Cheng HM (2003) J Am Chem Soc 125:3450
175. Shi HT, Qi LM, Ma JM, Wu NZ (2005) Adv Funct Mater 15:442
176. Manoli F, Dalas E (2000) J Cryst Growth 218:359
177. Qi LM, Ma JM (2002) Chem J Chin Univ 23:1595
178. Dickinson SR, Mcgrath KM (2003) J Mater Chem 13:928
179. Falini G, Gazzano M, Ripamonti A (1996) Chem Commun 1037
180. Seo KS, Han C, Wee JH, Park JK, Ahn JW (2005) J Cryst Growth 276:680
181. Chen SF, Yu SH, Yu B (2004) Chem Eur J 10:3050
182. Chen SF, Yu SH, Jiang J, Li FQ, Liu YK (2006) Chem Mater 18:122
183. Qi LM, Li J, Ma JM (2002) Chem J Chin Univ 23:1595

184. Naka K, Tanaka Y, Chujo Y (2002) Langmuir 18:3655
185. Kašparová P, Antonietti M, Cölfen H (2004) Colloids Surf A 250:153
186. Guo XH, Yu SH, Cai GB (2006) Angew Chem Int Ed 45:3977
187. Heywood BR (1996) Template-directed nucleation and growth of inorganic materials. In: Mann S (ed) Biomimetic materials chemistry. Wiley, New York, pp 143–173
188. Lowenstam HA (1981) Science 211:1126
189. Mann S, Heywood BR, Rajam S, Birchall JD (1988) Nature 334:692
190. Rajam S, Heywood BR, Walker JBA, Mann S, Davey RJ, Birchall JD (1991) J Chem Soc Faraday Trans 87:727
191. Heywood BR, Rajam S, Mann S (1991) J Chem Soc Faraday Trans 81:735
192. Heywood BR, Rajam S, Mann S (1992) J Am Chem Soc 114:4681
193. Heywood BR, Mann S (1992) Langmuir 8:1492
194. Heywood BR, Mann S (1992) Adv Mater 4:278
195. Fendler JH, Meldrum FC (1995) Adv Mater 7:607
196. Yang J, Fendler JH (1995) J Phys Chem 99:5505
197. Yang J, Fendler JH (1995) J Phys Chem 99:5500
198. Lahiri J, Xu G, Dabbs DM, Yao N, Aksay IA, Groves JT (1997) J Am Chem Soc 119:5449
199. Lahiri J, Fate GF, Ungashe SB, Groves JT (1996) J Am Chem Soc 118:2347
200. Han YJ, Aizenberg J (2003) Angew Chem Int Ed 42:3668
201. Travaille AM, Kaptijn L, Verwer P, Hulsken B, Elemans JAAW, Nolte RJM, van Kempen H (2003) J Am Chem Soc 125:11571
202. Han YJ, Laura M, Wysocki LM, Thanawala MS, Siegrist T, Aizenberg J (2005) Angew Chem Int Ed 44:2386
203. Davis SA, Burkett SL, Mendelson NH, Mann S (1997) Nature 385:420
204. Meldrum FC, Seshadri R (2000) Chem Commun 29
205. Yang D, Qi LM, Ma JM (2002) Adv Mater 14:1543
206. Cook G, Timms PL, Goeltner-Spickermann C (2003) Angew Chem Int Ed 42:557
207. Hall SR, Bolger H, Mann S (2003) Chem Commun 2784
208. Valtchev V, Smaihi M, Faust AC, Vidal L (2003) Angew Chem Int Ed 42:2782
209. Shin Y, Wang C, Exarhos GJ (2005) Adv Mater 17:73
210. Zhang DY, Qi LM (2005) Chem Commun 2735
211. Huang J, Kunitake T (2003) J Am Chem Soc 125:11834
212. Shin Y, Li XS, Wang C, Coleman JR, Exarhos GJ (2004) Adv Mater 16:1212
213. Falvo MR, Washburn R, Superfine R, Finch M, Brooks FP Jr, Chi V, Taylor RM II (1997) Biophys J 72:1396
214. Watson JD (1954) Biochim Biophys Acta 13:10
215. Knez M, Bittner AM, Boes F, Wege C, Jeske H, Mai E, Kern K (2003) Nano Lett 3:1079
216. Shenton W, Douglas T, Young M, Stubbs G, Mann S (1999) Adv Mater 11:253
217. Fowler CE, Shenton W, Stubbs G, Mann S (2001) Adv Mater 13:1266
218. Whaley SR, English DS, Hu EL, Barbara PF, Belcher AM (2000) Nature 405:665
219. Mao C, Flynn CE, Hayhurst A, Sweeney R, Qi J, Georgiou G, Iverson B, Belcher AM (2003) Proc Natl Acad Sci USA 100:6946
220. Lee SW, Mao CB, Flynn CE, Belcher AM (2002) Science 296:892
221. Mao C, Solis DJ, Reiss BD, Kottmann ST, Sweeney RY, Hayhurst A, Georgiou G, Iverson B, Belcher AM (2004) Science 303:213
222. Bogoyavlenskiy VA, Chernova NA (2000) Phys Rev E 61:1629
223. Busch S (1998) Dissertation, Technische Universität Darmstadt
224. Busch S, Dolhaine A, Duchesne A, Heinz S, Hochrein O, Laeri F, Podebrad O, Vietze U, Weiland T, Kniep R (1999) Eur J Inorg Chem 10:1643

225. Simon P, Zahn D, Lichte H, Kniep R (2006) Angew Chem Int Ed 45:1911
226. Cölfen H, Antonietti M (2005) Angew Chem Int Ed 44:5576
227. Putnis A, Prieto M, Fernandez-Diaz L (1995) Geol Mag 132:1
228. Zhan JH, Lin HP, Mou CY (2003) Adv Mater 15:621
229. Imai H, Oaki Y (2004) Angew Chem Int Ed 43:1363
230. Oaki Y, Imai H (2003) Cryst Growth Des 3:711
231. Sugawara A, Ishii T, Kato T (2003) Angew Chem Int Ed 42:5299
232. Gehrke N, Nassif N, Pinna N, Antonietti M, Gupta HS, Cölfen H (2005) Chem Mater 17:6514
233. Oaki Y, Imai H (2004) J Am Chem Soc 126:9271
234. Oaki Y, Imai H (2005) Langmuir 21:863
235. Oaki Y, Imai H (2005) Angew Chem Int Ed 44:6571
236. Oaki Y, Imai H (2005) Adv Funct Mater 15:1407
237. Oaki Y, Imai H (2005) Chem Commun 6011
238. Dalas E, Klepetsanis P, Koutsoukos PG (1999) Langmuir 15:8322
239. Lakshminarayanan R, Valiyaveettil S, Loy GL (2003) Cryst Growth Des 3:953
240. Nassif N, Gehrke N, Pinna N, Shirshova N, Tauer K, Antonietti M, Cölfen H (2005) Angew Chem Int Ed 44:6004
241. Lu CH, Qi LM, Cong HL, Wang XY, Yang JH, Yang LL, Zhang DY, Ma JM, Cao WX (2005) Chem Mater 17:5218
242. Walsh D, Lebeau B, Mann S (1999) Adv Mater 11:324
243. Park HK, Lee I, Kim K (2004) Chem Commun 24
244. Gao YQ, Yu SH, Cong HP (2006) Langmuir 22:6125
245. Aizenberg J, Black AJ, Whitesides GM (1999) Nature 398:495
246. Briseno AL, Aizenberg J, Han YJ, Penkala RA, Moon H, Lovinger AJ, Kloc C, Bao ZN (2005) J Am Chem Soc 127:12164
247. Aizenberg J, Muller DA, Grazul JL, Hamann DR (2003) Science 299:1205
248. Aizenberg J, Hendler G (2004) J Mater Chem 14:2066
249. Yang S, Chen G, Megens M, Ullal CK, Han YJ, Rapaport R, Thomas EL, Aizenberg J (2005) Adv Mater 17:435